NANOSTRUCTURAL METAL COMPOSITES: SYNTHESIS, STRUCTURAL AND THERMAL CHARACTERIZATION

A THESIS SUBMITTED TO
THE GRADUATE SCHOOL OF NATURAL AND APPLIED SCIENCES
OF
MIDDLE EAST TECHNICAL UNIVERSITY

BY

TUĞBA ORHAN

IN PARTIAL FULFILLMENT OF THE REQUIREMENTS
FOR
THE DEGREE OF MASTER OF SCIENCE
IN
CHEMISTRY

JULY 2009

Approval of the thesis:

NANOSTRUCTURAL METAL COMPOSITES: SYNTHESIS, STRUCTURAL AND THERMAL CHARCTERIZATION

submitted by **TUĞBA ORHAN** in partial fulfillment of the requirements for the degree of **Master of Science in Chemistry Department, Middle East Technical University** by,

Prof. Dr. Canan Özgen _____
Dean, **Graduate School of Natural and Applied Sciences**

Prof. Dr. Ahmet M. Önal _____
Head of Department, **Chemistry**

Prof. Dr. Ceyhan Kayran _____
Supervisor, **Chemistry Department, METU**

Prof. Dr. Jale Hacaloğlu _____
Co- Supervisor, **Chemistry Department, METU**

Examining Committee Members:

Prof. Dr. Zuhal Küçükyavuz _____
Chemistry Dept., METU

Prof. Dr. Ceyhan Kayran _____
Chemistry Dept., METU

Prof. Dr. Jale Hacaloğlu _____
Chemistry Dept., METU

Prof. Dr. Ayşen Yılmaz _____
Chemistry Dept., METU

Assoc. Prof. Dr. Tamer Uyar _____
UNAM, Bilkent Üniversitesi

Date: 16 July 2009

.

I hereby declare that all information in this document has been obtained and presented in accordance with academic rules and ethical conduct. I also declare that, as required by these rules and conduct, I have fully cited and referenced all materials and results that are not original to this work.

Name, Last name: Tuğba Orhan

Signature:

ABSTRACT

NANOSTRUCTURAL METAL COMPOSITES: SYNTHESIS, STRUCTURAL AND THERMAL CHARCTERIZATION

Orhan, Tuğba

M. Sc., Department of Polymer Science and Technology

Supervisor: Prof. Dr. Ceyhan Kayran

Co-Supervisor: Prof. Dr. Jale Hacaloğlu

July 16, 78 pages

Recently, the use of block copolymers in preparation of nanocomposites has received great attention as they form well-defined micelles.

In this work, the synthesis of different metal functional copolymers, nano structural metal composites and investigation of their reaction mechanism and thermal characteristics by pyrolysis mass spectroscopy have been aimed. Namely, polyisoprene-block-poly2vinylpyridine, (PI-b-P2VP) and poly2vinylpyridine-block-polymetylmethacrylate, (PMMA-b-P2VP) were used as block copolymers and the thermal reaction of these copolymers with two different transition metal complexes $Cr(CO)_6$ and $HAuCl_4.3H_2O$ were investigated which mostly lead to the coordination of metal through nitrogen atom of the pyridine ring which then degrates to form nano particles. The samples were further characterized by TEM, ATR-FT-IR, UV-Vis and Direct-Pyrolysis Mass Spectroscopy techniques.

TEM images proved the formation of nanoparticles and the results showed that synthesized Au nanoparticles have 2 to 3 fold larger size than Cr nanoparticles.

ATR-FT-IR spectrum of metal functional copolymers showed that the disappearance of characteristic peaks of pyridine stretching and bending mode when metal coordinates to the pyridine nitrogen. Furthermore, the spectrum indicated the appearance of a new absorption peak at around 740 cm^{-1} which may be a clue for the coordination of gold(III) ion to the pyridine nitrogen. Different from chromium case, in the spectrum of Au^{3+}-(PMMA-b-P2VP), CO stretching frequency of PMMA which may appear at around 1720–1718 cm^{-1} decreased in intensity while a new absorption peak appeared at around 1600 cm^{-1}. This results reveals that electron deficient gold (III) ion prefers the coordination from both donor atoms namely carbonyl oxygen PMMA and pyridine nitrogen of P2VP in order to compensate its electron deficiency.

In the UV-Vis spectrum of copolymers, Cr-functional copolymers showed a sharp absorption peak appeared at around 290 nm is attributed to a MLCT transition from chromium atom to π^* orbital of pyridine group. Furthermore, Au-functional copolymers showed a completely new absorption band at around 320 nm which can be associated again with a LMCT transition since gold is electron deficient and more willing to accept electrons from the ligand.

Pyrolysis mass spectrometry analysis showed that poly2vinylpyridine blocks for each copolymers were affected similarly but polyisoprene block was not affected much from the coordination of metal compared to poly(methyl methacrylate) block in copolymers. For (PI-b-P2VP), Au^{3+} coordination to copolymer resulted in the higher thermal stability compared to Cr coordination. For (PMMA-b-P2VP), different from Cr, Au^{3+} coordination to P2VP nitrogen atom was extensive and

PMMA based products changed drastically due to the coordination of electron deficient Au^{3+} to PMMA carbonyl group.

Keywords: Organometallic Polymer, Nano Structural Metal Composites, Pyrolysis

ÖZ

NANO YAPILI METALİK KOMPOZİTLER: SENTEZİ, YAPISAL VE ISIL KARAKTERİZASYONU

Orhan, Tuğba

Yüksek Lisans, Kimya Bölümü

Tez Yöneticisi: Prof. Dr. H. Ceyhan Kayran

Ortak Tez Yöneticisi: Prof. Dr. Jale Hacaloğlu

Temmuz 2009, 78 sayfa

Son zamanlarda, iyi tanımlanmış misel oluşturdukları için blok kopolimerlerin kullanımı büyük dikkat çekmiştir.

Bu çalışmada, farklı metal fonksiyonlu kopolimerlerin sentezi, nano yapılı metal kompozitler ve reaksiyon mekanizmaları ve ısısal karakteristiklerinin piroliz kütle spektroskopisiyle incelenmesi amaçlanmıştır. Poliizopren-blok-poli(2-vinilpiridin), (PI-b-P2VP) and poli(2-vinylpyridine-blok-polimetilmetakrilat, (PMMA-b-P2VP) adlı polimerler blok kopolimerler olarak kullanılmıştır ve bu kopolimerlerin iki farklı metal kompleksleri ile $Cr(CO)_6$ ve $HAuCl_4.3H_2O$, çoğunlukla metalin piridin halkasının nitrojen atomuna koordinasyonuyla sonuçlanması sonrası nano parçacıklar oluşturmak üzere degrade olmasının ısısal reaksiyonları incelenmiştir. Numuneler ayrıca TEM, ATR-FT-IR, UV-vis and direkt piroliz kütle spectroskopi teknikleri kullanılarak karakterize edilmiştir.

TEM görüntüleri nano parçacık oluşumunu kanıtlamıştır ve sonuçlar sentezlenen Au nano parçacıkları boyutunun Cr nano parçacıkları boyutundan 2–3 kat daha büyük olduğunu göstermiştir.

Metal fonksiyonlu kopolimerlerin ATR-FT-IR spektrumu, metal piridin nitrojenine koordine olduğunda piridin gerilme ve kırılma modlarının karakteristik piklerinin kaybolduğunu göstermiştir. Ayrıca, spektrum metal iyonunun piridin nitrojenine koordinasyonuna bir ipucu olabilecek yeni bir absorbsiyonun ortaya çıktığını göstermiştir. Krom durumundan farklı olarak, Au^{3+}-(PMMA-b-P2VP) spektrumunda, yeni bir absorbsiyon piki açığa çıkarken PMMA CO gerilme frekansının şiddeti azalmıştır ki bu eksik elektronlarını kompanse etmek için eksik elektronlu Au^{3+} her iki verici gruba, PMMA'nın karbonil oksijenine ve P2VP'nin piridin nitrojenine, koordinasyonu tercih ettiğini ortaya çıkarmaktadır.

Kopolimerlerin UV-vis spektrumunda, Cr-fonksiyonel kopolimerleri krom atomundan piridin grubunun π^* orbitalellerine MLCT geçişiyle ilişkilendirilen keskin bir absorbsiyon piki göstermiştir. Ayrıca, Au-fonksiyonel kopolimerleri altın eksik elektronlu ve liganttan elektron almaya daha istekli olduğundan LMCT geçişine ilişkilendirilebilecek tamamen yeni bir absorbsiyon bantı göstermiştir.

Piroliz kütle spektrometre analizi, Cr ve Au^{3+} metal ve metal iyonlarının her iki kopolimerin P2VP bloğunun piridin ünitesinin nitrojenine koordinasyonunun ısısal davranışı hemen hemen benzer şekilde etkilediğini göstermiştir. Genel olarak, Au^{3+} 'nun kopolimere koordinasyonu, Cr koordinasyonu için saptanılanla karşılaştırıldığında ısısal kararlılığı daha etkili bir şekilde arttırmıştır. (PMMA-b-P2VP) durumunda Au^{3+}'nın P2VP nitrojen atomuna yoğun bir

şekilde koordinasyonun yanı sıra, eksik elektronlu Au^{3+} 'nun PMMA'nın carbonil grubuna coordinasyonunun, PMMA bazlı ürünlerlerin ısısal kararlılıklarında şiddetli değişiklikle sonuçlandığı saptanmıştır.

Anahtar Kelimeler: Organometalik Polimer, Nano Yapılı Metal Kompozit, Piroliz

To my family, especialy to my dear father……

ACKNOWLEDGEMENTS

I would like to express my deep and sincere gratitude to my advisor Prof. Dr. Ceyhan Kayran. Her wide knowledge and her logical way of thinking have been of great value for me. Her understanding, encouraging and personal guidance have provided a good basis for the present thesis. I am deeply grateful to my co-advisor Prof. Dr. Jale Hacaloğlu, for her detailed and constructive comments, and for her important support throughout this work.

I owe many thanks to my lab partners, Meryem Karabulut and Shahla Bagherifam who always ready to give a hand whenever I needed. I truly thank to my dearest friends Ebru Ünel, Zafer Öztürk and Berrin Özkan who were with me in this sometimes challenging process to share their valuable comments and finally of course Erkunt Karabulut for his endless help for computer skills and his friendship.

I wish to express my sincere appreciation to Önder Metin for his support, answering my never ending questions and guidance to improve my skills during my study.

I am forever grateful to Ömer Lekesiz for his patience, support and belief in me. It makes me feel an extraordinarily lucky person to know that he was, is and will be there for me whenever I call for help.

Lastly, my deepest gratitude goes to my beloved parents and brother who always supported me and believed in me. Without their, especially my father's encouragement and immeasurable sacrifice, I could never finish this journey.

TABLE OF CONTENTS

ABSTRACT……..……..…….iv

ÖZ……..…….....……...vii

ACKNOWLEDGEMENTS……..…….…….....xi

TABLE OF CONTENTS……...…….……..xii

LIST OF TABLES……...……xvi

LIST OF FIGURES…….……xvii

LIST OF SCHEMES…….xxi

LIST OF SYMBOLS……xxii

CHAPTERS

1. INTRODUCTION……..……..…1

    1.1. Nano structural metal composites……....1

    1.2. Block copolymers in nanocomposites……..….4

    1.3. Aim ……....8

2. BONDING AND CHARACTERIZATION…….……...10

    2.1. Bonding…….....10

        2.1.1. Metal-carbonyl bonding…….....10

        2.1.2. Metal-halide bonding…..……..……11

        2.1.3. Metal-pyridine bonding…..……..……12

    2.2. Characterization…..……..…...13

        2.2.1. UV-Vis Analysis…….…….....13

        2.2.2. ATR-FT-IR Analysis…….……..15

        2.2.3. Thermal Analysis…….…….16

3. EXPERIMENTAL…….....18

    3.1. Basic Techniques…,……..……...18

    3.2. Chemicals…..……..……...20

    3.3. Synthesis of the Complexes…….....21

3.3.1. Synthesis of Chromium Poly(isoprene-block-vinyl-2-pyridine)…....22
3.3.2. Synthesis of Gold Poly (isoprene-block-vinyl-2-pyridine)…….....23
3.3.3. Synthesis of Chromium Poly(vinyl-2-pyridine-block-methyl methacrylate) ……..…...23
3.3.4. Synthesis of Gold Poly(vinyl-2-pyridine-block-methylmethacrylate)…….....23
3.4. Characterization.. ……..……..24
3.4.1. Transmission Electron Microscopy.. …….....24
3.4.2. UV-Vis Spectra……..……..24
3.4.3. ATR-FT_IR Spectra…..……..……24
3.4.4. Direct Pyrolysis Mass Spectrometry……..…..24
4. RESULTS AND DISCUSSION……..…….....25
4.1. Transmission Electron Microscopy…..……..……26
4.1.1. Chromium polyisoprene-block-poly(2-vinylpyridine), Cr-(PI-b-P2VP) …….....27
4.1.2. Gold polyisoprene-block-poly(2-vinylpyridine), Au-(PI-b-P2VP) ……...…...….28
4.1.3. Chromiumpoly(2-vinylpyridine)-block-poly(methyl methacrylate), Cr-(PMMA-b-P2VP) ……..……29
4.1.4. Gold poly(2-vinylpyridine)-block-poly(methyl methacrylate), Au- (PMMA-b-P2VP) ……..……..……...30
4.2. UV-Vis Characterization……..…...31
4.2.1.$HAuCl_4.3H_2O$…….31
4.2.2.$Cr(CO)_6$……..….32
4.2.3.Polyisoprene-block-poly(2-vinylpyridine), PI-b-P2VP…….…….....32

a. Chromium polyisoprene-block-poly(2-vinylpyridine), Cr-(PI-b-P2VP)…….……..33
b. Gold polyisoprene-block-poly(2-vinylpyridine), Au-(PI-b-P2VP)……...…….. 34
4.2.4.Poly(methyl methacrylate)-block-poly(2-vinylpyridine), PMMA-b-P2VP……....35
a. Chromium poly(methyl methacrylate)-block-poly(2-vinylpyridine), Cr- (PMMA-b-P2VP)…… .35
b. Goldpoly(methyl methacrylate)-block-poly(2-vinylpyridine), Au- (PMMA-b-P2VP)……...…..36
4.3. ATR-FT-IR Characterization…..…….....37
4.3.1.Polyisoprene-block-poly(2-vinylpyridine), PI-b-P2VP…….....37
a. Chromium polyisoprene-block-poly(2-vinylpyridine), Cr-(PI-b-P2VP)…….……38
b. Gold polyisoprene-block-poly(2-vinylpyridine), Au-(PI-b-P2VP)……....39
4.3.2.Poly(methyl methacrylate)-block-poly(2-vinylpyridine), PMMA-b-P2VP…….….40
a. Chromium poly(methyl methacrylate)-block-poly(2-vinylpyridine), Cr- (PMMA-b-P2VP)…….……40
b. Goldpoly(methyl methacrylate)-block-poly(2-vinylpyridine), Au- (PMMA-b-P2VP)……...……..41
4.4. Thermal Characterization of the Metal Copolymers.... ……...….……....43
4.4.1. Cr and Au^{3+} functional Poly(isoprene)-block-poly(2- vinyl pyridine)…….....43
4.4.1.1. Cr- (PI-b-P2VP).... …….……...51
4.4.1.2. Au^{3+} -(PI-b-P2VP).... ……...…..…55

4.4.2. Cr and Au^{3+} functional Poly(methyl methacrylate)-block-poly(2-vinylpyridine).... …….....60

4.4.2.1. Cr-(PMMA-b-P2VP).....……..….64

4.4.2.2. Au-(PMMA-b-P2VP).....…….....67

5. CONCLUSIONS.....……...73

REFERENCES…….....76

LIST OF TABLES

Table 2.1 Typical chromophores in spectroscopic data commonly found for polymers……..…….……14

Table 2.2. Table of Group Frequencies for Organic Species……..……...16

Table 3.1. The Reactants used and the Synthesized Product……...…...…….22

Table 4.1. Peak assignments for PI-b-P(2-VP)……..…..49

Table 4.2. Peak assignments for Cr PI-b-P2VP …….……..52

Table 4.3. Peak assignments for Au- PI-b-P2VP ……...……..57

Table 4.4. Peak assignments for (PMMA-b-P2VP)…….……..……..62

Table 4.5. Peak assignments for Cr- (PMMA-b-P2VP) …….65

Table 4.6. Peak assignments for Au-(PMMA-b-P2VP)……...……69

LIST OF FIGURES

Figure 1.1. Steric stabilization……...……..2

Figure 1.2. Ligand stabilization……...……...3

Figure 1.3. Formation of micelle for a A-B block copolymer……..……...6

Figure 1.4. a. The Open Structure of Polyisoprene-block-Poly(2-vinylpyridine)…....8

b. Coordination of PI-b-P2VP to the Transition Metal through Pyridine Nitrogen Atom. …….……8

Figure 1.5. a. The Open Structure of Poly(methyl methacrylate)-block-Poly(2-vinyl pyridine) ……..……9

b. Coordination of (PMMA-b-P2VP) to the Transition Metal through Pyridine Nitrogen Atom……..……...……9

Figure 2.1. Molecular Orbital Description of Metal Carbonyl Interaction……..……11

a. The formation of carbon to metal σ-bond, 'σ-dative interaction'

b. The formation of metal to carbon π-bond, 'π-back bonding'

Figure 2.2. Metal Halide Bonding……12

Figure 2.3. Metal– pyridine bonding interactions……...…..13

a. σ - interaction

b. π – interaction

Figure 3.1. Nitrogen and Argon Gas Purification System…….……19

Figure 3.2. Standard Schlenk Tube and Schlenk Flask……...……..……..20

Figure 3.3. The Apparatus Used During the Thermal Reaction. ……..…...21

Figure 4.1. TEM images of Cr-(PI-b-P2VP) ……..……27

Figure 4.2. TEM images of Au-(PI-b-P2VP) ……...……28

Figure 4.3. TEM images of Cr-(PMMA-b-P2VP) ……..……..……...29

Figure 4.4. TEM images of Au-(PMMA-b-P2VP) ……..…....30

Figure 4.5. UV-Vis spectra of Cr- (PI-b-P2VP), $Cr(CO)_6$,

(PI-b-P2VP)……33

Figure 4.6. UV-Vis spectra of Au-(PI-b-P2VP), $HAuCl_4$,

(PI-b-P2VP)…….34

F.gure 4.7. UV-Vis spectra of Cr-(PMMA-b-P2VP), $Cr(CO)_6$,

(PMMA-b-P2VP) ……...…...36

Figure 4.8. UV-Vis spectra of Au- (PMMA-b-P2VP), $HAuCl_4$,

P(PMMA-b-P2VP)…….....37

Figure 4.9. ATR-FT-IR Spectra of (PI-b-P2VP), Cr-(PI-b-P2VP)……..……38

Figure 4.10. ATR-FT-IR Spectra of (PI-b-P2VP), Au-(PI-b-P2VP)…….……39

Figure 4.11. ATR-FT-IR Spectra (PMMA-b-P2VP), Cr-(PMMA-b-P2VP)……....41

Figure 4.12. ATR-FT-IR Spectra of (PMMA-b-P2VP), Au-(PMMA-b-P2VP)……..42

Figure 4.13. The TIC curve and the pyrolysis mass spectra recorded during pyrolysis of PI-b-P2VP……..47

Figure 4.14 . Single ion evolution profiles of some selected thermal decomposition products recorded during the pyrolysis of PI-b-P2VP……...….50

Figure 4.15. The TIC curve and the pyrolysis mass spectra recorded during pyrolysis of Cr-(PI-b-P2VP)…….…….....…51

Figure 4.16. Single ion evolution profiles of some selected thermal decomposition products recorded during the pyrolysis of Cr-PI-b-P2VP…….....54

Figure 4.17. The TIC curve and the pyrolysis mass spectra recorded during pyrolysis of Au-PI-b-P2VP……..56

Figure 4.18. Single ion evolution profiles of some selected thermal decomposition products recorded during the pyrolysis of Au-PI-b-P2VP……...……58

Figure 4.19. The TIC curve and the pyrolysis mass spectra recorded during pyrolysis of PMMA-b-P2VP……...…….61

Figure 4.20. Single ion evolution profiles of some selected thermal decomposition products recorded during the pyrolysis of PMMA-b-P2VP…….……..63

Figure 4.21. The TIC curve and the pyrolysis mass spectra recorded during pyrolysis of Cr-PMMA-b-P2VP……..64

Figure 4.22. Single ion evolution profiles of some selected thermal decomposition products recorded during the pyrolysis of Cr-PMMA-b-P2VP…....…66

Figure 4.23. The TIC curve and the pyrolysis mass spectra recorded during pyrolysis of Au-(PMMA-b-P2VP). ……..….68

Figure 4.24. Single ion evolution profiles of some selected thermal decomposition products recorded during the pyrolysis of Au-PMMA-b-P2VP…...…72

LIST OF SCHEMES

Scheme 4.1. H-transfer reactions generating $(VP)_x$, $[(VP)_x\text{-H}]$ and pyridine…….....44

Scheme 4.2 Thermal degradation mechanism of polyisoprene ……...46

Scheme 4.3 Thermal degradation mechanism of metal-coordinated copolymer…..55

Scheme 4.4. Thermal degradation mechanism of poly(methyl methacrylate)……..60

Scheme 4.5. Thermal degradation mechanism of metal-coordinated PMMA Block……..71

LIST OF SYMBOLS

π = pi orbital

π^* = pi star orbital

σ = sigma orbital

n$\rightarrow \pi$ = from nonbonding to pi orbital

$\pi \rightarrow \pi^*$ = from pi to pi star orbital

λ_{max} = Alpha maximum

ϵ_{max} = Molar absorptivity constant

CHAPTER 1

INTRODUCTION

The metal functional nano composites have been the subject of several studies because of their outstanding properties and wide application areas.

1.1. Nano structural metal composites

Today's material science deals increasingly with nanostructures, i.e., with structures of characteristic dimension between 1 and 100 nm. An important goal of materials science is the controlled and specific synthesis of well-defined nanostructures as well as nano and mesoporous materials. [1]

Nanoclusters are small particles of metal, metal oxides or semiconductor materials that posses interesting and useful catalytic, magnetic, optical, electronic and chemical properties. These materials often display properties intermediate between the bulk and the atom, which are the result of size quantization effects as well as of the high number of surface atoms with special surface states. Those properties can be controlled through the immobilization and the assembly of nanoparticles on an appropriate substrate or in a suitable medium. Further, the clusters must be stabilized against aggregation and growth to maintain the performance of the composite material. [1-3]

Because of their small size, nanoparticles have a very high surface area/volume ratio resulting in a high reactivity and the need for stabilization. When particles are not

stabilized they will generally undergo a process known as Ostwald Ripening. Ostwald Ripening describes the tendency for smaller particles to merge into one another until one large particle remains. To avoid this, various stabilizers are used. Previously, they were low-molecular organic compounds (carbonic acids, alcohols, amides) and natural polymers (gelatin, starch, cellulose and so on). At present more frequently synthetic polymers are employed. They solve the problems of nanoparticle stabilization and introduction of a polymer ingredient into the nanocomposite.

Figure 1.1. given below shows how a gold (Au) nanoparticle can be stabilized sterically by coating it with a layer of polymer or protein. This layer keeps the particle from aggregating with neighboring particles.

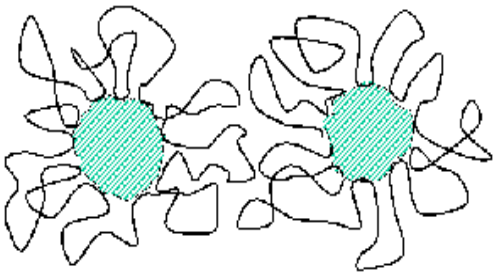

Figure 1.1. Steric stabilization

By attaching ligands with a negatively charged end group to the particles a repulsive force between the particles is introduced to keep them form coming in contact with one another.

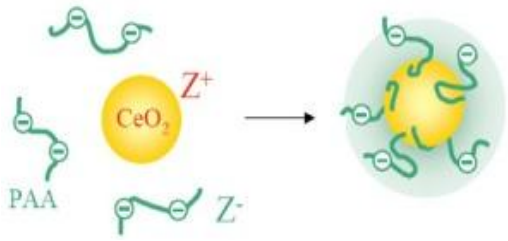

Figure 1.2. Ligand stabilization [4]

Stabilization of metal-containing clusters can be achieved by using alkane thiols, micelle surfactants and polymers. [5]

For building up smaller structures, nature may serve as a model, where by self-organization and building up compartments, individual molecules are integrated into larger functional units and structural hierarchies. One single self-organization step is often not sufficient to realize functional systems. Several hierarchy levels can be distinguished for block copolymers as well, their characteristic lengths ranging from 1 nm up to 1 mm.

1.2. Block copolymers in nanocomposites

The monomers defining the chemical functionality are on the smallest length scale. Living or controlled polymerization processes lead to the formation of block copolymers. The simplest block copolymers are linear diblock copolymers, which are comprised of two distinct polymer chains covalently connected at their endpoints to form a chain. Their block lengths and block length ratios define a local

length scale and a local symmetry. The long range repulsion and the short range attraction result in microphase separation, for example the formation of a micelle. This is the stage in which micro-compartments and interfaces form with typical length scales between 10–100 nm. These micro-compartments can act as hosts for sequestering nanoscopic inclusions of appropriate chemical affinity and geometry.

Based on the volume fraction of the microphases and the local geometry of the interface, different superlattices can form the degree of order and the orientation being determined by application of macroscopic fields.

Using block copolymers enables structure control to be carried out at every stage of hierarchy:

1) Via the block lengths the aggregation number and the size of the micelle are directly controlled,

2) Depending on the volume fraction of the block copolymer there is a formation of well-defined superlattices in lyotropic phases or in the solid.

3) External mechanical or electric fields can result in a macroscopic orientation of the superlattices.[1]

Microphase separation in pure block copolymers is a well-studied phenomenon producing morphologies by phase separation that are determined by the relative lengths of the polymer blocks, ranging from spheres to lamellae, or interconnected network morphologies.[6]

The size of each block of the polymer domain is determined by its overall chain length, thus providing a wide range of self-organized nanoscale- level templates. Most importantly, microphase-separated block copolymers spontaneously self-assemble into regular arrays of domains whose size can be controlled from a few to several tens of nanometers, and in turn can act as hosts for sequestering nanoscopic inclusions of appropriate chemical affinity and geometry. Thus, block copolymers can be used as templates to provide supramolecular control over the size, particle density, and spatial location of various inorganic nanoparticles. [3]

The synthesis of metal clusters in microcompartments of self-organized polymer systems offers the advantage to restrict the size growth of the particles to a predefined diameter and to prevent the particles from further aggregation. If the microcompartments are arranged on a superlattice, the synthesis leads the nanoparticles to become also integrated into the lattice. This gives rise to the formation of nanostructured inorganic/polymer hybrid materials. The extremely large inorganic/polymer interface can be stabilized by attaching appropriate ligands to the polymer blocks. Weakly coordinated metal complexes serve as precursor materials which, by complex formation with the ligands, can be solubilized into the polymer compartments. There should not be too strong complexation between the

precursor and the ligand; as otherwise, there will be no further reaction with the elementary metal. [1-9]

Self-assembly of A-B block copolymer in dilute solutions forms well-defined micelles, being well suited for the preparation of nanostructures as the size and the shape of these micelles depend only on the block molecular weights and the solvent used, not on the concentration. [8]

Block copolymer micelles have a well-defined core–shell structure with a core consisting of the insoluble A blocks and a shell or corona of the soluble B blocks.

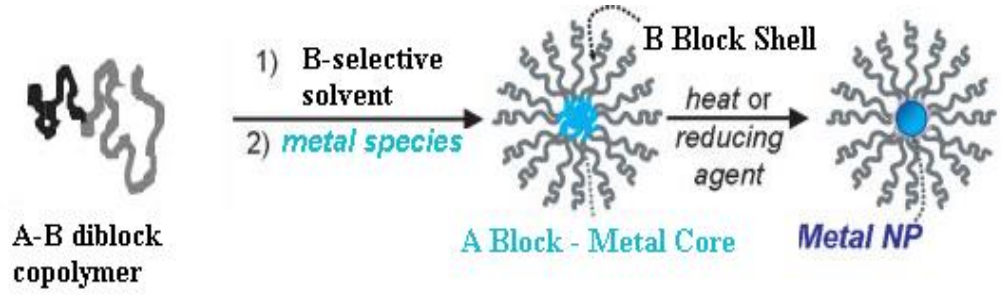

Figure1.3. Formation of micelle for a A-B block copolymer

For the preparation of the metal nanaoparticles, specialty monomers with phosphine and thioether ligands were used in the earliest approaches; however, poly(vinylpyridine) (PVP) is currently the most common block used in coordination approaches.

Recently, methods of synthesizing nanoclusters in micro-phase separated diblock copolymers having polyvinylpyridine blocks have been reported that provide greater control over cluster formation [10-14].

For example, Moeller and co-workers [15, 16] has prepared gold nanoparticles with the use of polystyrene-block-poly-2-vinylpyridine (PS-b-P2VP) copolymer for the first time. The metal salts formed complexes with the pendant pyridine rings, concentrating the metal ions in the poly-2-vinylpyridine domains.

Though several studies on preparation and application of these important materials have been carried out, the knowledge of reaction mechanism and thermal characteristics that are very important for investigation of synthesis routes and application areas are still limited. Among several thermal analysis methods, pyrolysis mass spectrometry (py-MS) is one of the methods that give information on not only thermal stability but also on thermal degradation products.

In the previous studies performed in our group, metal functional copolymers, namely Cr-PS-b-P2VP, Co-PS-b-P2VP, Au-PS-b-P2VP, Fe-PS-b-P2VP and Mo-PS-b-P2VP were prepared. TEM images indicated the formation of Au^{III}, Cr and Co nanoparticles. Furthermore, crystalline structures were detected for Fe-PS-b-P2VP and Mo-PS-b-P2VP. FT-IR analysis supported the formation of metal-nitrogen bond. On the other hand, direct pyrolysis mass spectrometry analysis showed an increase in the thermal stability of P2VP chains involving metal or metal ion coordination to pyridine units. The thermal stability of these chains increased in the order Co< Cr <Au^{3+} indicating a stronger coordination in the same order [17]. In an other study of our group, the analysis of Co nanoparticles with PS-b-P4VP was also performed and both TEM and pyrolysis mass spectrometry results indicated that PS-b-P2VP is a better matrix for metal bonding for which the particle distribution is much better and more effective than PS-b-P4VP polymer[18].

1.3. Aim

In the present work, the synthesis and characterization of different nano structural metal functional copolymers and investigation of their reaction mechanism and thermal characteristics by pyrolysis mass spectrometry have been aimed. For this reason, different copolymers involving again P2VP blocks were chosen, namely, polyisoprene-block-poly(2-vinylpyridine), PI-b-P2VP (Figure 1.4) and poly(methyl methacrylate)-block-poly(2-vinylpyridine), PMMA-b-P2VP (Figure 1.5) to investigate the effect of noncoordinating block on structural and thermal characteristics of the nanocomposites prepared. The thermal reaction of these copolymers with two different transition metal complexes $Cr(CO)_6$ and $HAuCl_4.3H_2O$ were performed. The samples prepared were characterized by ATR-FT-IR, UV-vis, direct pyrolysis mass spectrometry and TEM.

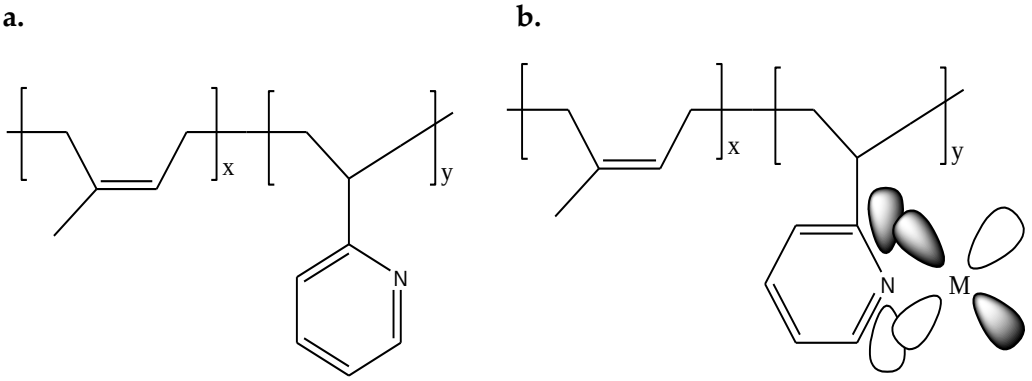

Figure 1. 4. a. The Open Structure of Polyisoprene-block-Poly(2-vinylpyridine).
b. Coordination of PI-b-P2VP to the transition metal through pyridine nitrogen atom.

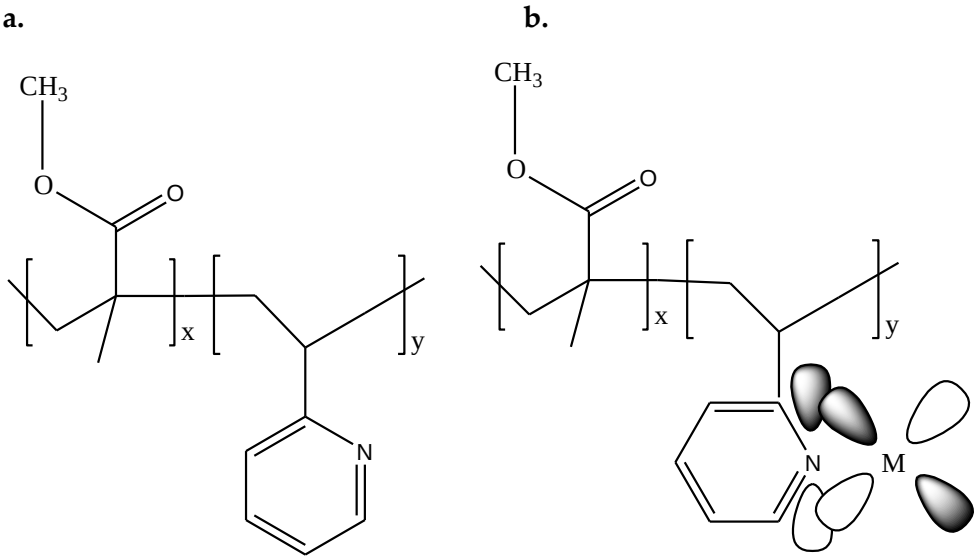

Figure 1.5. a. The Open Structure of Poly(metyl methacrylate)-block-poly(2-vinylpyridine).

b. Coordination of PMMA-b-P2VP to the transition metal through pyridine nitrogen atom.

CHAPTER 2

BONDING AND CHARACTERIZATION

2.1. Bonding

2.1.1. Metal-carbonyl bonding

Carbonyl complexes are compounds that contain carbon monoxide as a coordinated ligand. Carbon monoxide is a common ligand in transition metal chemistry, in part due to the synergistic nature of its bonding to transition metals. The bonding of CO to a metal can be described as consisting of two components.

The first component is a two electron donation of the lone pair on carbon (coordination exclusively through the oxygen is extremely rare) into a vacant metal d-orbital. This electron donation makes the metal more electron rich, and in order to compensate for this increased electron density, a filled metal d-orbital may interact with the empty π^* orbital on the carbonyl ligand to relieve itself of the added electron density. This second component is called π-backbonding or π-backdonation.

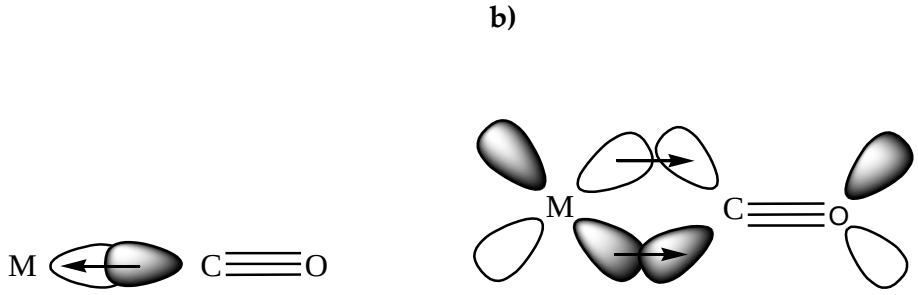

Figure 2.1. Molecular Orbital Description of Metal Carbonyl Interaction

a. The formation of carbon to metal σ-bond, 'σ-dative interaction'
b. The formation of metal to carbon π-bond, 'π-back bonding'

The π-bonding has the effect of weakening the carbon-oxygen bond compared with free carbon monoxide. Because of the multiple bond character of the M-CO linkage, the distance between the metal and carbon is relatively short. [19, 20].

2.1.2. Metal-halide bonding

The halides are known to be π donor ligand when coordinated to the metal. Halides lone pairs are donated to the metal atom through π bonding and they are classified as weakly coordinating ligands but good leaving groups. As a result, when metal salts such as hydrogen tetrachloroaurate(III) trihydrate reacts with the copolymers, the halide ligand leaves the coordination sphere of the complex and copolymers coordinate to the metal through pyridine nitrogen atom.[21,22]

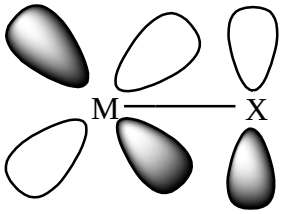

Figure 2.2. Metal Halide Bonding

2.1.3. Metal-pyridine bonding

Polyvinyl pyridine is one of the common blocks in the block copolymers that self-assembled into different nanostructures. The metal salts form complexes with the pendant pyridine rings, concentrating the metal ions in the poly-2-vinylpyridine domains. The nitrogen atom in the pyridine ring has sp^2 orbitals containing only one electron and overlaps with metal d orbital of σ symmetry ($d_{x^2-y^2}$) and donates

electron to form a σ bond. On the other hand, the p orbital of nitrogen (containing one electron) perpendicular to the plane of the ring is capable of accepting an electron from metal d orbitals (d_{xz} and d_{yz}). The donation of the lone-pair electrons on the nitrogen atom of the pyridine molecule is the major contribution to the binding interaction between pyridine and each metal cluster. The back-donation interaction from the metal atoms to the π-type anti-bonding orbital is very weak in all these complexes [23]. As a conclusion, one can assume that pyridine is a σ-donor and π-acceptor ligand. The thermal reaction of the metal complexes with the copolymers containing viniylpyridine block proceeds through the coordination of pyridine nitrogen atom to the corresponding metal (Figure 1.8) which then degredates to form nanoparticles.

a) **b)**

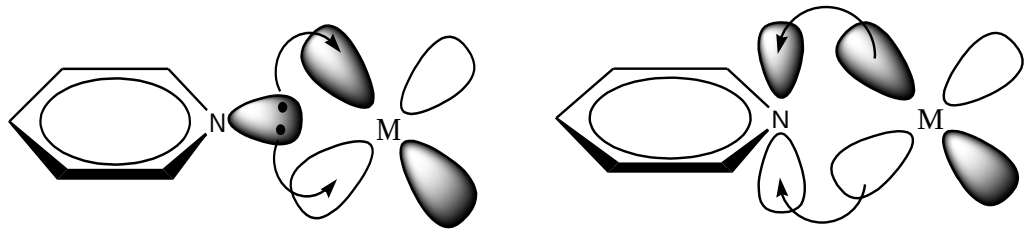

Figure 2.3. Metal– pyridine bonding interactions

a) σ - interaction

b) π – interaction

2.2. Characterization

2.2.1. UV-Vis Analysis

The absorption of ultraviolet or visible radiation by polymers leads to transitions among the electronic energy levels or an electronic absorption spectrum results. UV-vis spectroscopy can be used to identify chromospheres such as benzene rings or carbonyl groups. *Chromophores* are functional groups responsible for electronic absorption, with that undergo n $\rightarrow \pi^*$ or $\pi \rightarrow \pi^*$ transitions. UV-vis spectroscopy is limited to polymers containing appropriate groups, including polymers with aromatic ring or carbonyl groups, or polyenes. In Table 2.1. typical chromophores in polymers are summarized.

Table 2.1 Typical chromophores in spectroscopic data commonly found for polymers

Chromophore	Wavelength, λ_{max} (nm)	Molar Absorptivity, ε_{max}
C = C	175	14 000
	185	8 000
C ≡ C	175	10 000
	195	2 000
	223	150
C = O	160	18 000
	185	500
	280	15
C = C – C = C	217	20 000
Benzene Ring	184	60 000
	200	4 400
	255	204

In inorganic chemistry, most charge-transfer complexes involve electron transfer between metal atoms and ligands. The charge-transfer bands in transition metal complexes result from movement of electrons between molecular orbitals (MO) that are predominantly metal in character and those that are predominantly ligand in character. If the electron moves from the MO with ligand like character to the metal like one, the complex is called ligand-to-metal charge-transfer **(LMCT)** complex. If the electron moves from the MO with metal like character to the ligand-like one, the complex is called a metal-to-ligand charge-transfer **(MLCT)** complex. Thus, a MLCT results in oxidation of the metal center whereas a LMCT results in the reduction of the metal center. [24]

2.2.2. ATR-ATR-FT-IR Analysis

FT-IR spectrometry is a versatile tool that is applied to the qualitative and quantitative analysis of molecular species of all types by highly accurate and reproducible frequency determinations. Identification of the species from a spectrum can be achieved by comparison of the frequencies with the correlation charts and group frequencies. Therefore, FT-IR spectrometry permits us to what functional groups are likely to be present or absent in a molecule. The mechanism of the reactions can also be determined by taking subsequent samples during the reaction. [24]. Internal-reflection spectroscopy is a technique for obtaining infrared spectra of samples that are difficult deal with, such as, solids of limited solubility, films, pastes and powders. Attenuated total reflectance spectra are similar but not identical to ordinary absorption spectra. In general, while the same peaks are observed, their relative intensities differ. The absorbances, while dependent on the angle of incidence, are independent of sample thickness, since radiation penetrates only a few micrometers into the sample. One of the major advantages of attenuated total reflectance spectroscopy is that absorption spectra are readily obtainable on a wide variety of sample types with a minimum of preparation. In Table 2.2. FT-IR data for selected groups are given.

Table 2.2. Table of Group Frequencies for Organic Species

Bond	Types of Compound	Frequency Range, cm^{-1}	Intensity
C-H	Alkanes	2850-2970	Strong
		1340-1470	Strong
	Aromatic rings		
		3010-3100	Medium
		690-900	Strong
C=C	Aromatic rings	1500-1600	Variable
C=O	Aldehydes, ethers, carboxylic acids, esters	1690-1760	Strong
C-O	Aldehydes, ethers, carboxylic acids, esters	1050-1300	Strong

2.2.3. Thermal Analysis

Among several thermal analysis methods thermal **gravimetry-FT-IR (TG-FT-IR), thermal gravimetry-mass spectrometry (TG-MS)** and **pyrolysis mass spectrometry (py-MS)** are the ones that give information not only on thermal stability but also on thermal degradation products that can be used to investigate mechanism.

Pyrolysis is thermal degradation of materials by cleavage at their weakest points to produce smaller volatile fragments in an inert atmosphere or vacuum. Pyrolysis is widely applied to investigate thermal characteristics of a compound such as, thermal stability, degradation products and decomposition mechanism. It is also used as a pre-processing step to convert large molecules into lower mass molecules that are easily detectable. For instance, when polymers are pyrolyzed, smaller fragments, oligomers, are produced and analysis of these fragments aids in the identification of the polymers.

Pyrolysis technique can be coupled with **FT-IR, GC (Py-GC), GC/MS (Py-GC/MS)** or **MS (DP-MS)**. Among these various analytical pyrolysis techniques, pyrolysis gas chromatography mass spectrometry, Py-GC-MS and direct pyrolysis mass spectrometry, DP-MS, have several advantages such as sensitivity, reproducibility, minimal sample preparation and consumption and speed of analysis**.**

Although py-GC-MS technique is significantly sensitive, only stable thermal degradation products can be detected with the use of this technique. On the other hand, DP-MS technique offers several advantages. The high vacuum inside the mass spectrometer favors vaporization and thus allows the analysis of higher molecular mass pyrolyzates. As the high vacuum system rapidly removes the degradation products from the heating zone, secondary reactions and condensation reactions are avoided. Furthermore, because of the rapid detection system of the mass spectrometers, unstable thermal degradation products can also be detected. [25-32]

CHAPTER 3

EXPERIMENTAL

3.1. Basic Techniques

Most of the organometallic compounds are air sensitive and may decompose unless handled properly. Organometallic complexes may be handled as easily as ordinary compounds, if the reactions are carried out in the absence of oxygen and water, for example under dry and deoxygenated nitrogen gas atmosphere as oxidation occurs at a significant rate at room temperature in many cases. For the preparation of deoxygenated nitrogen, nitrogen gas is allowed to pass through diphosphorus pentoxide (P_2O_5), and then deoxygenated by using a catalyst and finally dried molecular sieves to remove its moisture before using in the reaction medium. Generally, the catalyst, cupper(I)oxide should be heated to 120 ^{0}C using an electrical resistance, and hydrogen gas should be passed through the system from time to time to regenerate the catalyst. (Figure 3 .1)

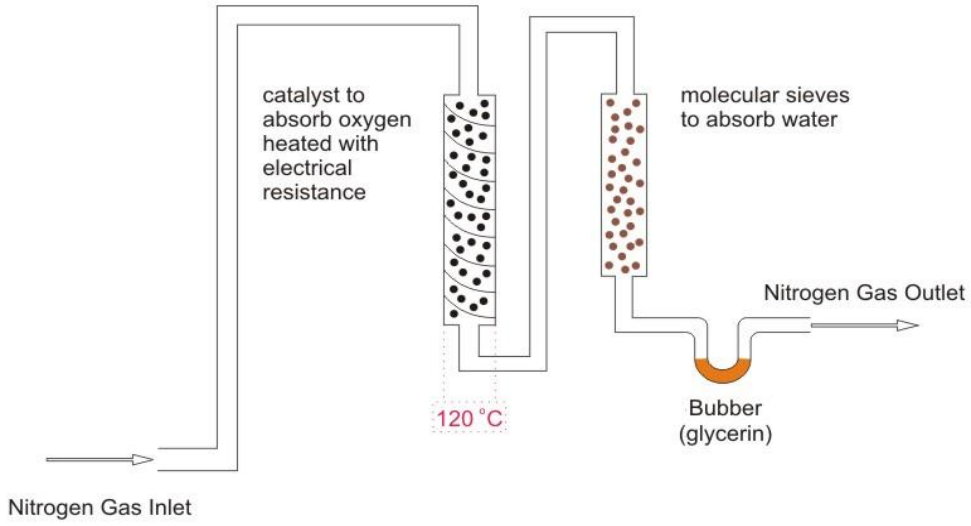

Figure 3.1. Nitrogen and Argon Gas Purification System

For carrying out experiments with exclusion of oxygen, schlenk technique can be used, in which a simple two-necked vessel, designed to permit passage of a nitrogen stream through the narrow neck with the stopcock while using the wider neck without stopcock for operations such as inserting a spatula for scraping or removal of material.

Figure 3.2. Standard Schlenk Tube and Schlenk Flask

3.2 Chemicals

The transition metal complexes $Cr(CO)_6$ and $HAuCl_4.3H_2O$ were purchased from Aldrich Chemical company and Acros Organics, respectively and used without further purification. Polyisoprene-block-poly(2-vinylpyridine) [MW = PI(76000)-b-P2VP(23500)] having polydispersity index 1.04 and poly(2-vinylpyridine)-block-poly(methyl methacrylate) [MW = PMMA(18700)-b-P2VP(4200)] having polydispersity index 1.09 were purchased from Polymer Sources, Inc. Toluene, the only solvent, purchased from Carlo Erba Reagenti was purified by refluxing over metallic sodium under nitrogen for two or three days.

3.3. Synthesis of the Complexes

All the complexes were synthesized applying the same procedure known from literature with some modification [33]. Table 3.1 lists the polymer and transition metal complexes used and the products obtained with the thermal reaction of metal complexes with two different copolymers. First, the polymer was dissolved in toluene by stirring overnight. After the dissolution of the polymer, the metal complex was added to this solution and refluxed for 8 hours. All of the reactions were performed by using two necked flask with a nitrogen connection as the synthesis of organometallic compounds is very sensitive to oxygen. After the synthesis of the complexes, solution was poured into a schlenk tube for toluene evaporation by vacuum. The solid remained was used for structural and thermal analysis.

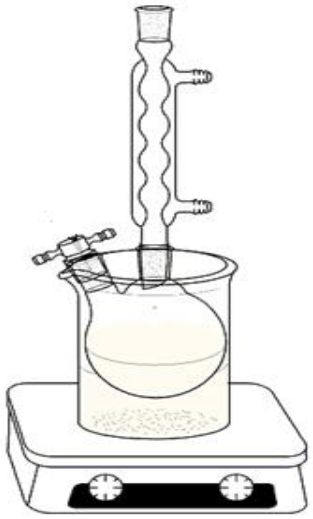

Figure 3.3. The Apparatus Used During the Thermal Reaction.

Table 3.1. The Reactants used and the Synthesized Product

Polymer	**Transition Metal Complexes**	**Product**
Polyisoprene-block-poly(2-vinylpyridine) **(PI-b-P2VP)**	Chromium hexacarnonyl **$Cr(CO)_6$**	**Cr- (PI-b-P2VP)**
	Hydrogen tetrachloroaurate(III) trihydrate **$HAuCl_4.3H_2O$**	**Au- (PI-b-P2VP)**
Poly(methyl methacrylate)-block-Poly(2-vinylpyridine) **(PMMA-b-P2VP)**	Chromium hexacarnonyl **$Cr(CO)_6$**	**Cr-(PMMA-b-P2VP)**
	Hydrogen tetrachloroaurate(III) trihydrate **$HAuCl_4.3H_2O$**	**Au-(PMMA-b-P2VP)**

3.3.1. Synthesis of Chromium Polyisoprene-block-poly(2-vinylpyridine)

103 mg (PI-b-P2VP) was dissolved totally in 15 mL toluene (bp: 108-109 ^{0}C). 257 mg $Cr(CO)_6$ was added to this solution. The mixture was refluxed under deooxygenated nitrogen atmosphere for 8 hours at the boiling point of toluene, at 110 ^{0}C. Finally, the solvent was evaporated under vacuum. The resultant product was analyzed by means of TEM, ATR-FT-IR, Uv-vis and direct pyrolysis mass spectrometry techniques.

3.3.2. Synthesis of Gold Polyisoprene-block-poly(2-vinylpyridine)

480 mg $HAuCl_4.3H_2O$ was added to a solution prepared by dissolving 103 mg (PI-b-P2VP) in 15 mL toluene. The mixture was refluxed for 8 hours at 110 ^{0}C under nitrogen atmosphere. Finally, the solvent was evaporated under vacuum and the resultant product was analyzed by means of TEM, ATR-FT-IR, Uv-vis and direct pyrolysis mass spectrometry techniques.

3.3.3. Synthesis of Chromium poly(methyl methacrylate)-block- poly(2-vinylpyridine)

135 mg (PMMA-b-P2VP) was dissolved totally in 15 mL toluene.. 257 mg $Cr(CO)_6$ was added to this solution. The mixture was refluxed under deooxygenated nitrogen atmosphere for 8 hours at the boiling point of toluene, at 110 ^{0}C. Finally, the solvent was evaporated under vacuum. The resultant product was analyzed by means of TEM, ATR-FT-IR, Uv-vis and direct pyrolysis mass spectrometry techniques.

3.3.4. Synthesis of Gold poly(methyl methacrylate)-block- poly(2-vinylpyridine)

480 mg $HAuCl_4.3H_2O$ was added to a solution prepared by dissolving 135 mg (PMMA-b-P2VP) in 15 mL toluene. The mixture was refluxed for 8 hours at 110 ^{0}C under nitrogen atmosphere. Finally, the solvent was evaporated under vacuum and the resultant product was analyzed by means of TEM, ATR-FT-IR, Uv-vis and direct pyrolysis mass spectrometry techniques

3.4. Characterization

3.4.1. Transmission Electron Microscopy

Transmission electron microscope (TEM) imaging of the nanoparticles was carried out with a FEI Tecnai G2 F30 instrument at 200 kV. The nanoparticles were dispersed on the carbon-coated grid from their diluted suspension of toluene. The syntheses of the metal nanoparticles were confirmed by TEM.

3.4.2. UV-Vis Spectra

The electron absorption spectra of the samples were recorded on a Varian Cary 100 Bio UV-Vis Spectrophotometer.

3.4.3. ATR-FT-IR Spectra

ATR-FT-IR analyses of the samples were performed by directly insertion of solid sample using Bruker Vertex 70 Spectrophotometer.

3.4.4. Direct Pyrolysis Mass Spectrometry

DP-MS analyses were made by using *Waters Micromass Quattro Micro GC Mass Spectrometer* with a mass range is 10 to 1500 Da and EI ion source *coupled to a Direct Insertion Probe*. During the pyrolysis the temperature was increased to 50 °C at a rate of 5 °C/ min., then was raised to 650 °C with a rate of 10 °C/min. and kept at 650 °C for 5 additional minutes while recording 70eV EI mass spectra at a mass scan rate of 1 scan/s. Deep capillary quartz tubes were used as sample containers.

CHAPTER 4

RESULTS AND DISCUSSION

The formation of metal nanoparticles by reacting organometallic precursors in solutions of copolymer aggregates is known from literature [34-37]. It is known that aggregations were generated upon formation of metal nanoparticles by reactions of organometallic precursors with copolymers in solutions. These have included solutions of block copolymers [38,39] and surfactants [40]. In the literature studies, in all systems, the coordinating species consisted of pendent moieties that were polar than the solvent system employed for particle formation [38]**.** The hypothesis was that the metal precursors coordinates with an electron- rich segment of the copolymer (Fig. 1.4 and Figure 1.5.) and, upon heating the copolymers displace the precursor ligands (e.g. carbon monoxide, halides etc) to afford metal nanoparticles encased in copolymer sheath. It is reasoned that this could result from diffusion of the metal precursor into the core of a copolymer micelle where coordination and then reaction takes place. The same strategy was used in the present work. The organometallic compounds or transition metal precursors, $Cr(CO)_6$, $HAuCl_4$ reacted thermally with (PI-b-P2VP), (PMMA-b-P2VP) for about 8 hours for the generation of metal functional copolymer. The metal functional copolymer formation starts by the coordination of the electron-rich segment of the copolymer that is 2-vinylpyridine part in the case of PI-b-P2VP) to the metal atom with the exclusion of the ligands. In

the case of PMMA-b-P2VP copolymer has two possible coordination side to the metal atom which are namely carbonyl oxygen on the PMMA part and pyridine nitrogen on the 2-vinylpyridine.

4.1. Transmission Electron Microscopy

The TEM images of four metal-functional polymers, Cr-(PMMA-b-P2VP), Cr-(PI-b-P2VP), Au^{3+}- (PMMA-b-P2VP) and Au^{3+}-(PI-b-P2VP) are shown in the below Figure 4.1. As can be noticed from the figures, gold nanoparticles have higher dimensions and more micelle like structures. Au nanoparticles are about 2-3 fold larger than Cr nanoparticles for both copolymers.

4.1.1. Chromium polyisoprene-block-poly(2-vinylpyridine), Cr-(PI-b-P2VP)

a. **b.**

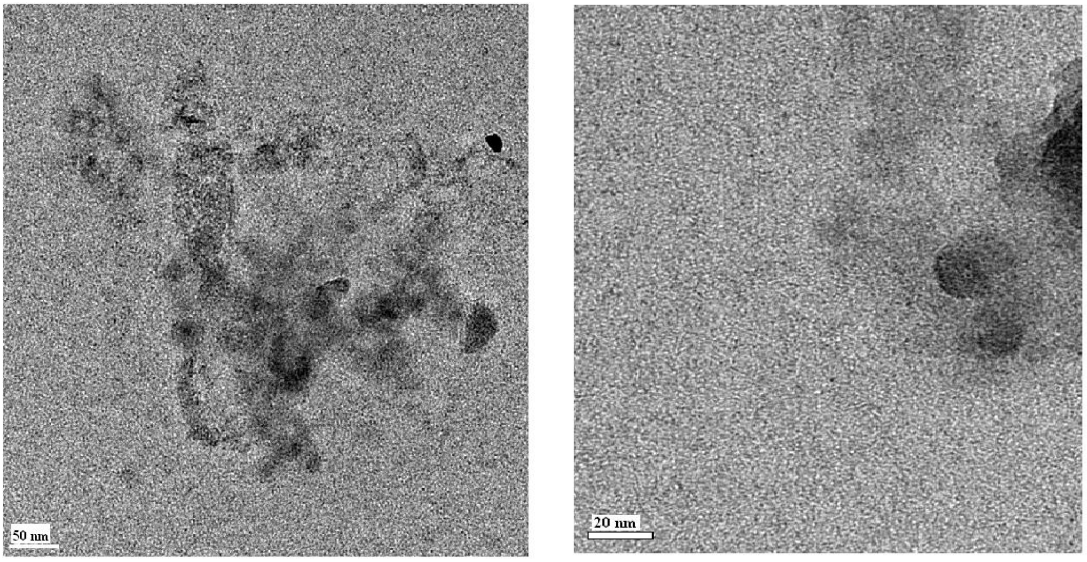

Figure 4.1. TEM images of Cr-(PI-b-P2VP)

a. 50 nm

b. 20 nm

4.1.2. Gold polyisoprene-block-poly(2-vinylpyridine), Au^{3+}-(PI-b-P2VP)

a. **b.**

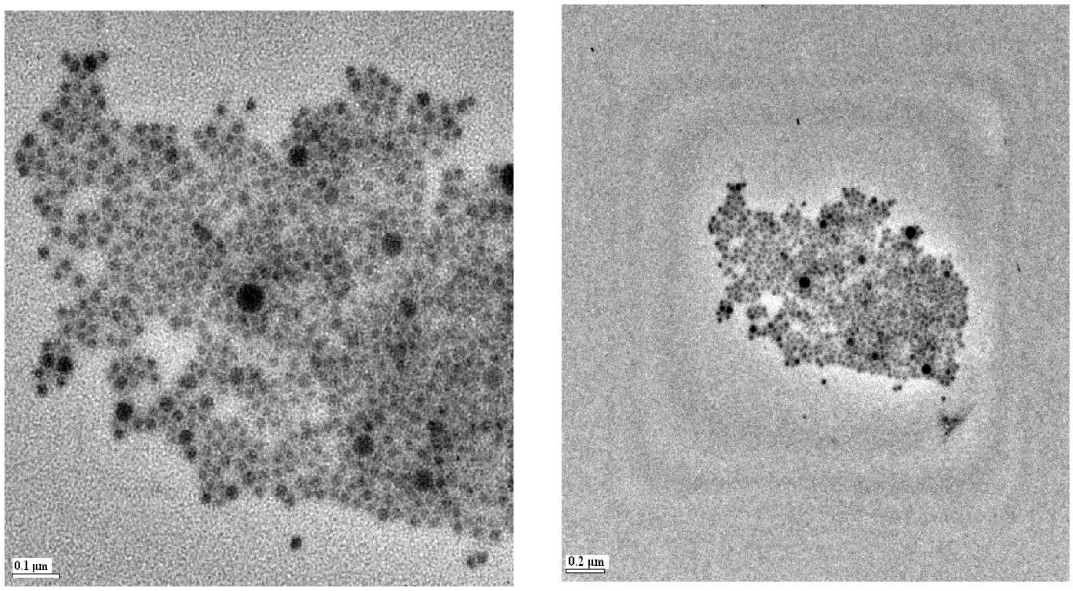

Figure 4.2. TEM images of Au^{3+}-(PI-b-P2VP)

a. 0.1 µm

b. 0.2 µm

4.1.3. Chromium poly(2-vinylpyridine)-block-poly(methyl methacrylate), Cr-(PMMA-b-P2VP)

a. **b.**

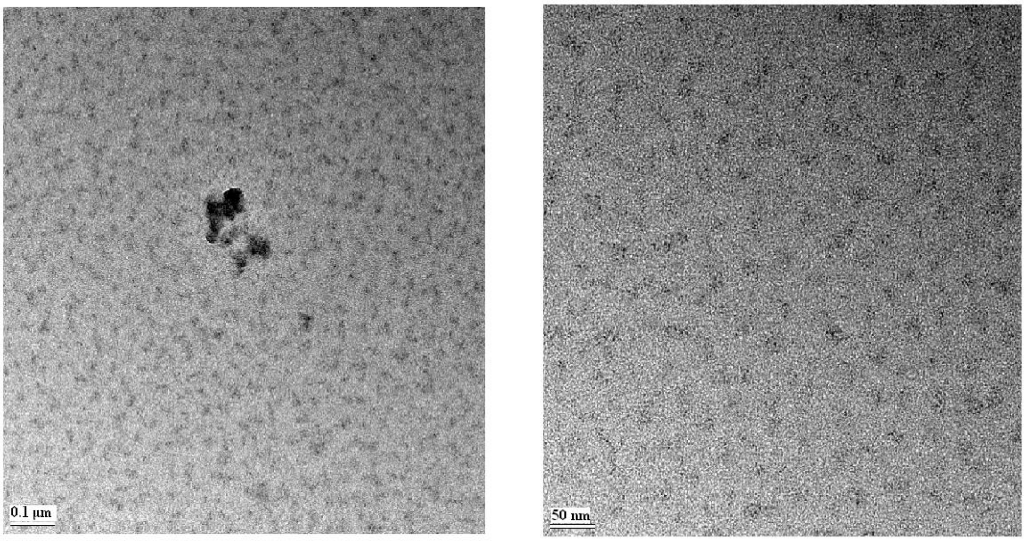

Figure 4.3. TEM images of Cr-(PMMA-b-P2VP)

a. 0.1 µm

b. 50 nm

4.1.4. Gold poly(2-vinylpyridine)-block-poly(methyl methacrylate), Au^{3+}-(PMMA-b-P2VP)

a. **b.**

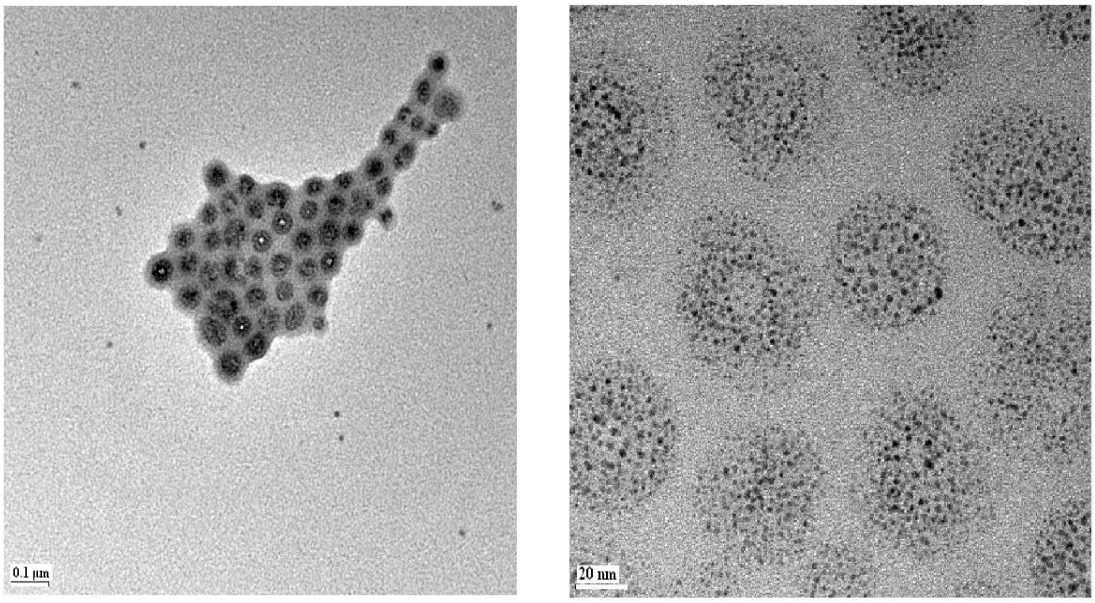

Figure 4.4. TEM images of Au^{3+}-(PMMA-b-P2VP)

a. 0.1 μm

b. 20 nm

4.2. UV-Vis Characterization

In order to characterize metal functional copolymers via UV-vis spectroscopy, the corresponding data for the reactants, $HAuCl_4.3H_2O$, $Cr(CO)_6$, PI-b-P2VP and PMMA-b-P2VP were investigated first.

4.2.1. $HAuCl_4.3H_2O$

The intense bands exhibited by many halo complexes in the UV region have been assigned as ligand-to-metal charge transfer (LMCT) electronic transitions. Such transitions involve excitation of electrons from occupied orbitals localized on the halide to an empty or partly filled orbital of predominantly metal character, commonly a metal d orbital. The LMCT transitions can thus be viewed as an incipient reduction of the metal with concomitant oxidation of the halide ligand and are therefore related to the redox properties of the metal ion and halide. As we all know, Au (III) with its d^8 electronic configuration forms a variety of square-planar complexes. Since Au^{III} is an oxidizing agent, low-energy LMCT transitions are quite important. However, for this complex, MLCT transitions do not exist due to the lack of reducing properties of Au(III). As in the case of most of the electronic spectra of various halide compounds of gold [21,22, 41-43], sometimes it may be difficult to make complete assignments of absorption peaks due to the complications caused by the appearance of LMCT and less intense LF bands in the same energy range.

Another important point is that as the oxidation number of the metal increases the electron accepting orbital of the metal that is $d_{x2-y2}(b_{1g})$ lowers in energy therefore the energy of the LMCT shifts to lower energy[44]. UV-vis spectrum of the square planar tetrachloroaurate (III) complex exhibits LMCT transitions at around 290 nm. A broad shoulder appears at around 400 nm may be attributed to spin forbidden LMCT transition. The less intense d-d transition may be under this broad LMCT band.

4.2.2. $Cr(CO)_6$

When one analyzes the UV-vis spectrum of of $Cr(CO)_6$, it is clearly seen that the most characteristic electron transfer is metal to ligand charge transfer transition (MLCT) observed at around 280 nm. Electron rich chromium atom donates electron to the low-lying π^* orbital of carbonyl ligand.

4.2.3. Polyisoprene-block-poly(2-vinylpyridine), PI-b-P2VP

PI-b-P2VP has two blocks namely, polyisoprene and poly(2-vinylpyridine). Polyisoprene block gives absorption bands due π to π^* excitation within the conjugated system present at around 278 nm. For poly(2-vinylpyridine) block, the characteristic absorption band appears at around 285 nm due to $n \rightarrow \pi^*$ excitation from the pyridine nitrogen lone pairs to the low-lying π^* orbitals of the pyridine ring.

a. Chromium polyisoprene-block-poly(2-vinylpyridine), Cr-(PI-b-P2VP)

In the UV-vis spectrum of the product Cr-(PI-b-P2VP), the sharp absorption peak appeared at around 290 nm is attributed to a MLCT transition from chromium atom to π^* orbital of pyridine group. A weak absorption band is also observed at around 320 nm originating from spin forbidden MLCT similar to the previous example(Figure 4.5.).

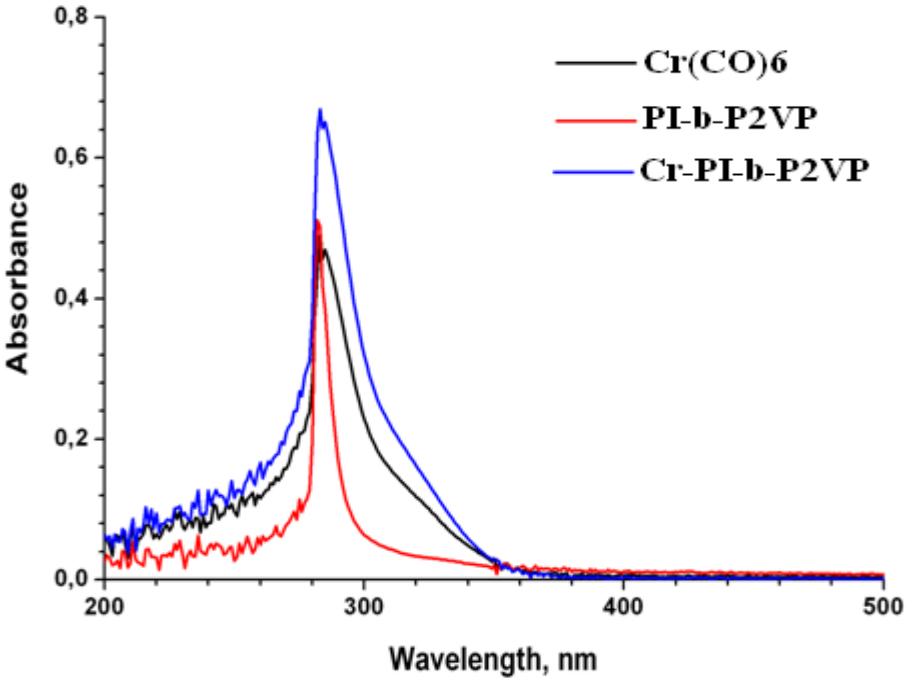

Figure 4.5. UV-Vis spectra of Cr- (PI-b-P2VP), $Cr(CO)_6$, PI-b-P2VP

b. Gold polyisoprene-block-poly(2-vinylpyridine), Au^{3+}-(PI-b-P2VP)

UV-vis spectrum of Au-(PI-b-P2VP) gives a completely new absorption band at around 320 nm which can be associated with a LMCT transition since gold is electron deficient and more willing to accept electrons from the ligand. When gold ion coordinates to pyridine nitrogen atom, nitrogen lone pair electrons are donated to the d orbitals of gold metal in order to overcome the electron deficiency of the gold (III) ion (Figure 4.6.).

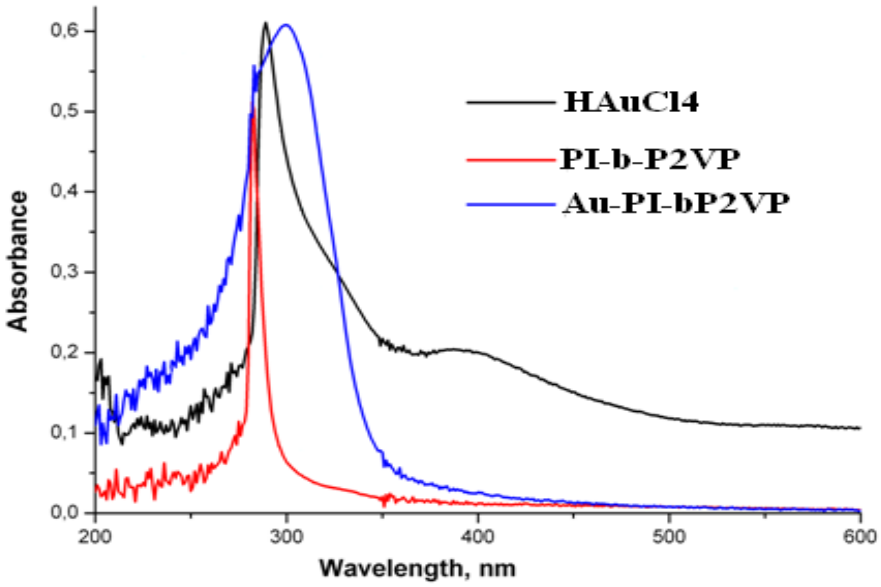

Figure 4.6. UV-Vis spectra of Au^{3+}-(PI-b-P2VP), $HAuCl_4$, (PI-b-P2VP)

4.2.4. Poly(methyl methacrylate)-block-poly(2-vinylpyridine), PMMA-b-P2VP

In the UV-vis spectrum of the copolymer P(2VP-b-MMA), as mentioned before, the 2-vinylpyridine block gives an absorption band at around 280 nm due to $n \rightarrow \pi^*$ transition since the lone pairs of pyridine nitrogen is donated to the low-lying π^* orbital of pyridine ring. PMMA block of the copolymer also gives absorption band at around 275–280 nm which overlapped with that of 2-vinylpyridine block. PMMA is a saturated aliphatic polymer with a carbonyl group as chromophore. The most typical absorption band for carbonyl compounds is that of $n \rightarrow \pi^*$ transition. The absorption peak overlapped with $n \rightarrow \pi^*$ transition band observed in the poly2-vinylpyrdine part of the copolymer.

a. Chromium poly(methyl methacrylate)-block-poly(2-vinylpyridine) Cr-(PMMA-b-P2VP)

In the UV-vis spectrum of the product Cr-P(2VP-b-MMA), the sharp absorption peak appeared at around 330 nm is attributed to a MLCT transition from chromium atom to π^* orbital of pyridine group. A weak absorption band is also observed at around 440 nm originating spin forbidden MLCT (Figure 4.7.).

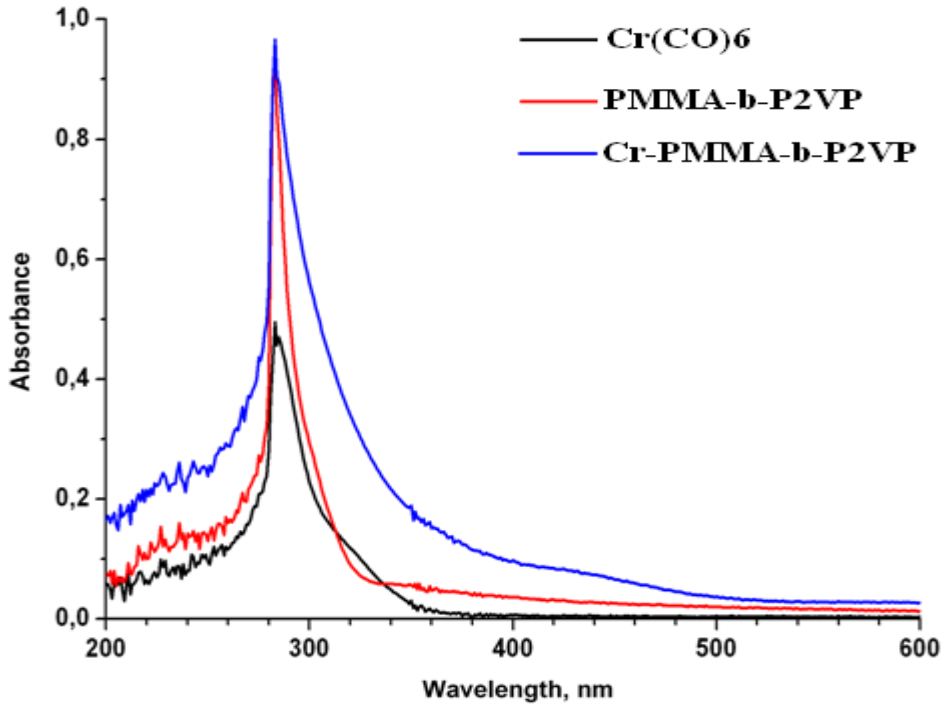

Figure 4.7. UV-Vis spectra of Cr-(PMMA-b-P2VP), $Cr(CO)_6$, PMMA-b-P2VP

b. Gold poly(methyl methacrylate), -block-poly(2-vinylpyridine), Au^{3+}- (PMMA-b-P2VP)

UV-vis spectrum of the square planar tetrachloroaurate (III), $HAuCl_4$, complex exhibits LMCT transitions at around 298 nm.

In the UV-vis spectrum of the product Au-(PMMA-b-P2VP) the sharp absorption band appeared at around 295 nm is attributed to a LMCT transition (donation of the lone pairs pyridine nitrogen to the low-lying metal d orbitals gold(III) ions). A shoulder, more intense compared to Cr-(PMMA-b-P2VP), was observed at around

330 nm which may be originating from the spin forbidden LMCT from pyridine nitrogen and also from carbonyl oxygen to the gold ion (Figure 4.8.).

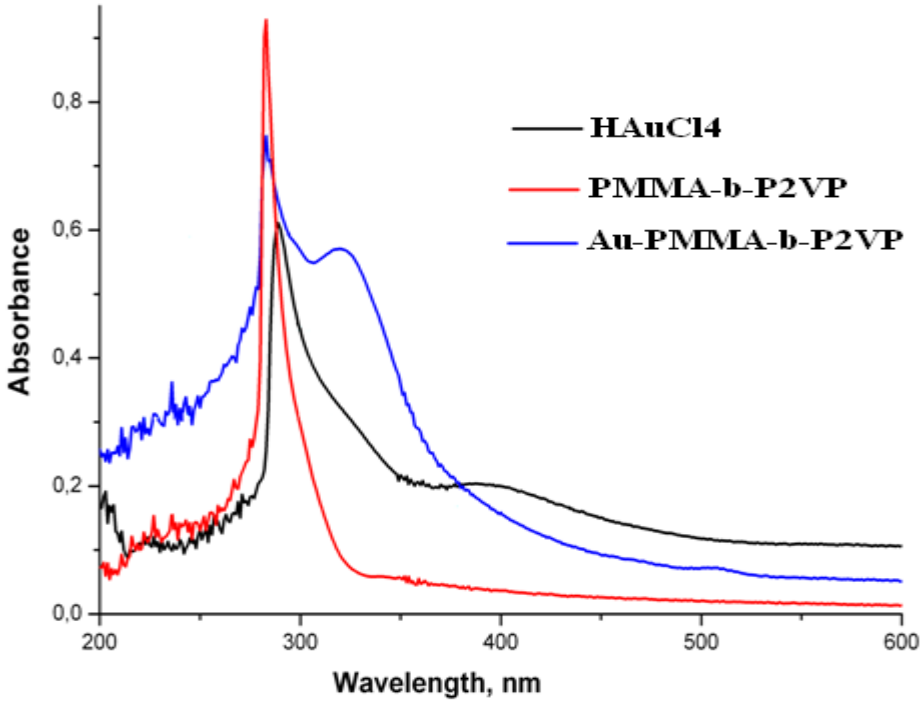

Figure 4.8. UV-Vis spectra of Au^{3+}-(PMMA-b-P2VP), $HAuCl_4$, PMMA-b-P2VP

4.3. ATR- FT-IR Characterization

4.3.1. Polyisoprene-block-poly(2-vinylpyridine), PI-b-P2VP

The ATR-FT-IR spectrum of polyisoprene-block-poly(2-vinylpyridine), PI-b-P2VP, shows the characteristic absorption peaks of P2VP blocks at around 1434–1030 cm^{-1}

for the C-H pyridine ring stretching mode[45]. In the polyisoprene block, =C-H stretching frequency comes around 3400 cm^{-1} which appears weak in intensity in olefinic compounds [46]. The absorption peak which comes around 2915 cm^{-1} may be due to CH_2 asymmetric stretching mode. CH_2 symmetric stretching mode of polyisoprene appears at around 1880 cm^{-1}.

a. Chromium polyisoprene-block-poly(2-vinylpyridine), Cr-(PI-b-P2VP)

Significant changes were detected in the ATR-FT-IR spectrum of Cr-(PI-b-P2VP) (Figure 4.9.) compared to that of the copolymer, PI-b-P2VP, mainly in the peaks associated with poly(2-vinylpyridine) block(Figure 4.9.). The absorption peaks appear in the range of 1730-1000 cm^{-1} due to the pyridine stretching and bending modes which decreased in intensity upon coordination to the metal. Especially, the shift for the C-N stretching mode from 1587 to 1718 cm^{-1} could be an evidence for the coordination of the chromium metal to the pyridine nitrogen.

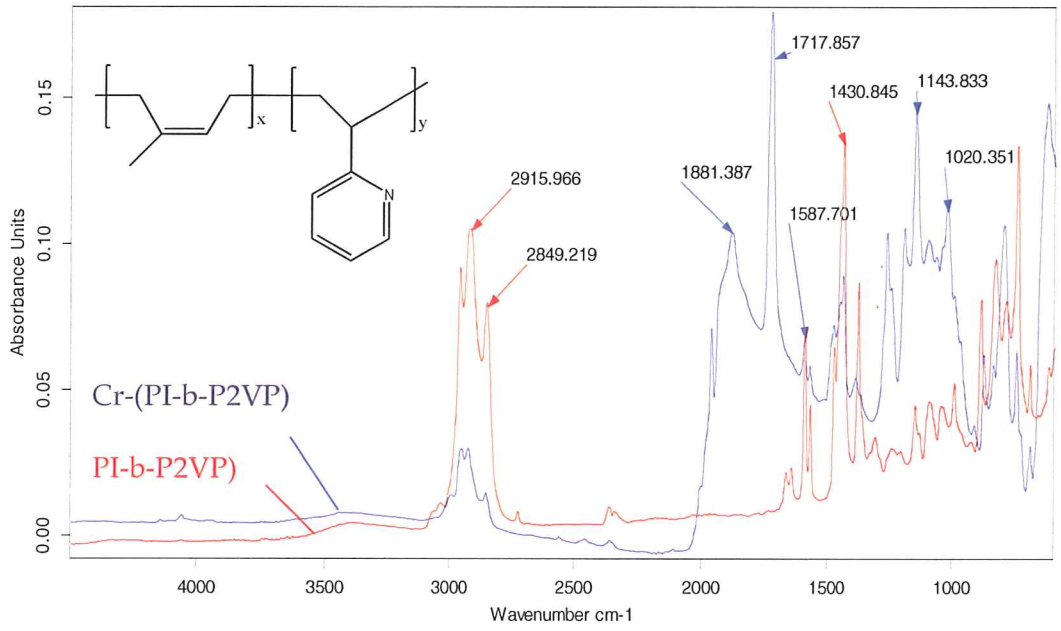

Figure 4.9. ATR-FT-IR Spectra of PI-b-P2VP, Cr-(PI-b-2VP)

b. Gold polyisoprene-block-Poly(2-vinylpyridine), Au^{3+}-(PI-b-P2VP)

When the ATR-FT-IR spectrum of the copolymer and that of Au-bonded copolymer are compared, the decrease in the pyridine stretching modes at 1430 cm^{-1} can be easily seen. The shift for the C-N stretching mode from 1587 to 1623 cm^{-1} can be attributed to the coordination of the metal. Furthermore, the coordinated pyridine ring stretching peaks shifted to 1017 cm^{-1}(Figure 4.10.).

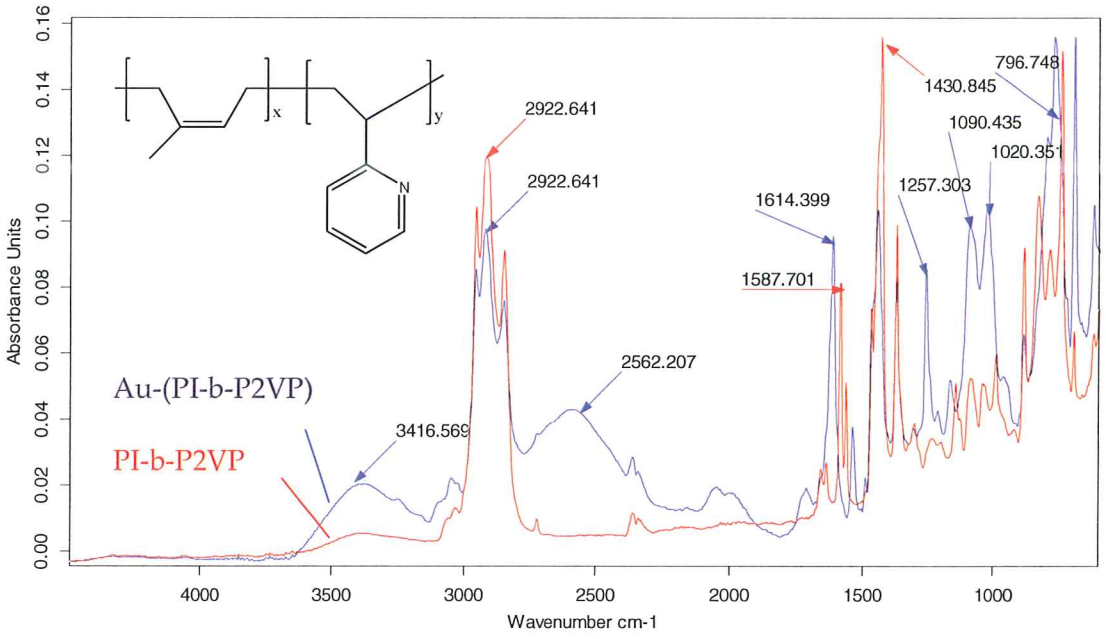

Figure 4.10. ATR-FT-IR Spectra of PI-b-P2VP), Au^{3+}-(PI-b-P2VP)

4.3.2. Poly(methyl methacrylate)-block-poly(2-vinylpyridine), PMMA-b-P2VP

The ATR-FT-IR spectrum of poly(methyl methacrylate)-block-poly(2-vinylpyridine), PMMA-b-P2VP shows the characteristic absorption peaks of P2VP blocks at around 1434–1030 cm^{-1} for the C-H pyridine ring stretching mode.

The PMMA which is a saturated polymeric ester, the C=O symmetrical stretching frequency gives rise to an intense very strong peak at around 1718 cm^{-1}. The absorption peak at around 1143 cm^{-1} can assigned to O-CH_3 deformation, O-C, C-O-C symmetric stretching of PMMA. The CH_3 asymmetric stretching vibration occurs at around 2920 cm^{-1}. The stretching vibration of CH_2 of PMMA appears at around 3500 cm^{-1} as a broad peak. [47]

a. Chromium poly(methyl methacrylate)-block-poly(2-vinylpyridine) Cr-(PMMA-b-P2VP)

Significant changes were detected in the ATR-FT-IR spectrum of Cr-(PMMA-b-P2VP) compared to that of the copolymer (Figure 4.11.). The relative intensities of the absorption peaks, in the range of 1500–600 cm^{-1}, especially, the ones at around 1145 cm^{-1} due to the pyridine stretching and bending modes are decreased significantly. For this sample the coordinated pyridine ring stretching peaks shifted to 1025 cm^{-1}.

On the other hand, the absorption peak due to ester carbonyl stretching vibration at round 1718 cm^{-1} seemed to be not affected much.

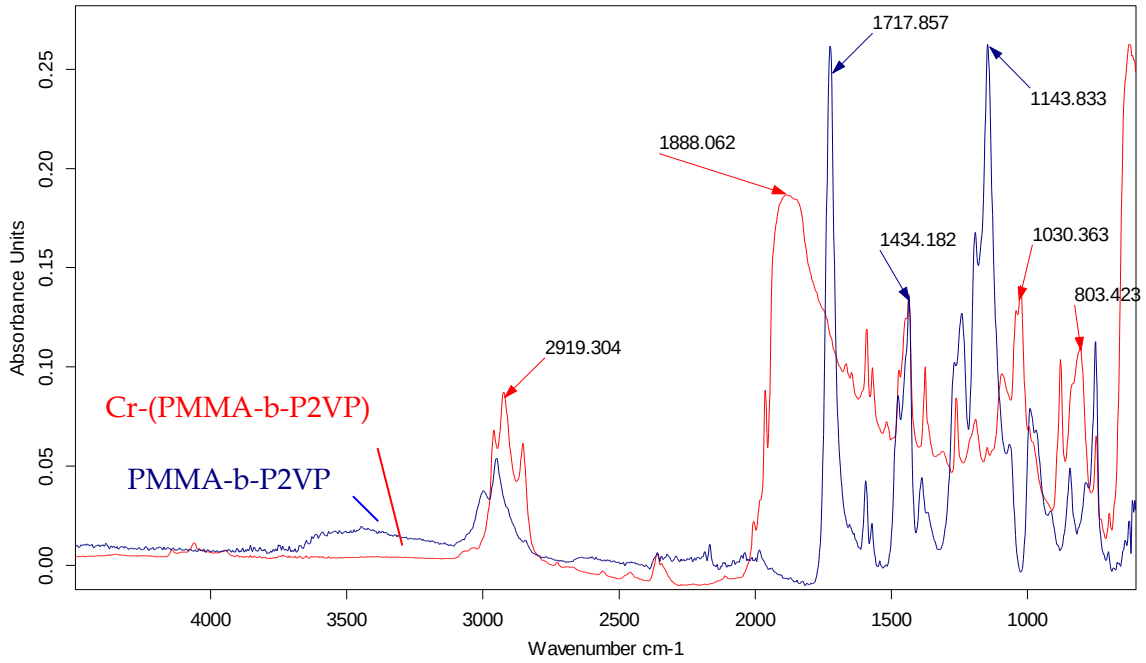

Figure 4.11. ATR-FT-IR Spectra of (PMMA-b-P2VP) and Cr-(PMMA-b-P2VP)

b. Gold poly(methyl methacrylate)-block-poly(2-vinylpyridine), Au^{3+}-(PMMA-b-P2VP)

The FT-IR spectrum of the Au coordinated PMMA-b-P2VP(Figure 4.12.) shows decrease in the pyridine stretching modes in the region 1145-1030 cm^{-1} as can be seen in Figure . The shift for the C-N stretching mode from 1590 to 1623 cm^{-1} can be attributed to the coordination of the gold ion to N. Again shift for the coordinated pyridine ring stretching peaks to 1040 cm^{-1} was detected. Different from the chromium case, in the case of gold (III) complex, CO stretching frequency of PMMA appeared at around 1720-1718 cm^{-1} decreased in intensity. This result reveals that

electron deficient gold (III) ion also preferred the coordination from both donor atoms of PMMA (namely carbonyl oxygen and pyridine nitrogen) in order to compensate its electron deficiency.

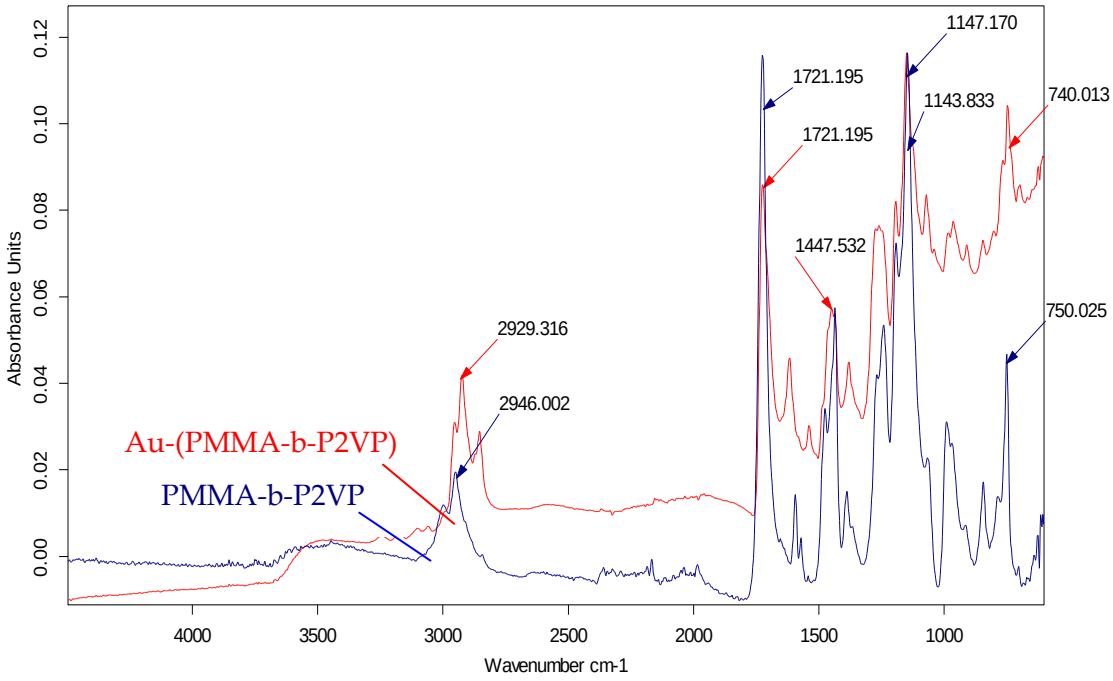

Figure 4.12. ATR-FT-IR Spectra of PMMA-b-P2VP, Au^{3+}-(PMMA-b-P2VP)

4.4. THERMAL CHARACTERIZATION OF THE METAL COPOLYMERS

Thermal characteristics of Cr and Au^{3+} functional copolymers were studied via direct pyrolysis mass spectrometry. Actually, the pyrolysis mass spectra of polymers are usually very complex as thermal degradation products further dissociate in the mass spectrometer during ionization. Furthermore, all the fragments with the same mass to charge ratio have contributions to the intensity of the same peak in the mass spectrum. Thus, in pyrolysis MS analysis, not only the detection of a peak but also the changes in its intensity (single ion pyrograms, evolution profiles) as a function of temperature have significant importance. For the case of copolymers thermal characteristics of both components have to be known for a better understanding.

4.4.1 Cr and Au^{3+} functional Polyisoprene-block-poly(2-vinylpyridine)

In order to investigate thermal characteristics of Cr and Au^{3+} functional polyisoprene-block-poly(2-vinylpyridine), the knowledge of thermal characteristics of the homopolymers and the virgin copolymer is necessary.

The thermal degradation of P2VP has been studied in detail in the literature[18]. It is known that P2VP degrades via radicallic depolymerization yielding mainly vinylpyridine monomer. Furthermore, loss of pyridine and proton transfer to N

atom yielding unsaturated linkages on the polymer backbone which in turn increases thermal stability as shown in Scheme 4.1. was proposed recently in the literature[18].

Scheme 4.1. H-transfer reactions generating $(VP)_x$, $[(VP)_x\text{-H}]$ and pyridine.

a. H-transfer to the chain ends

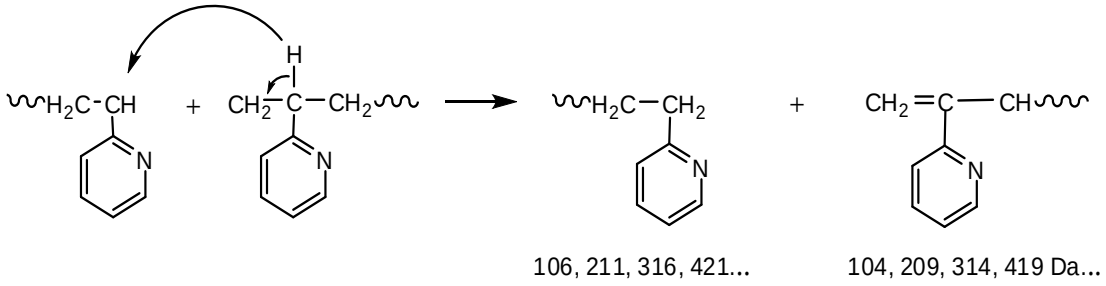

b. H-transfer to N atom in the pyridine ring

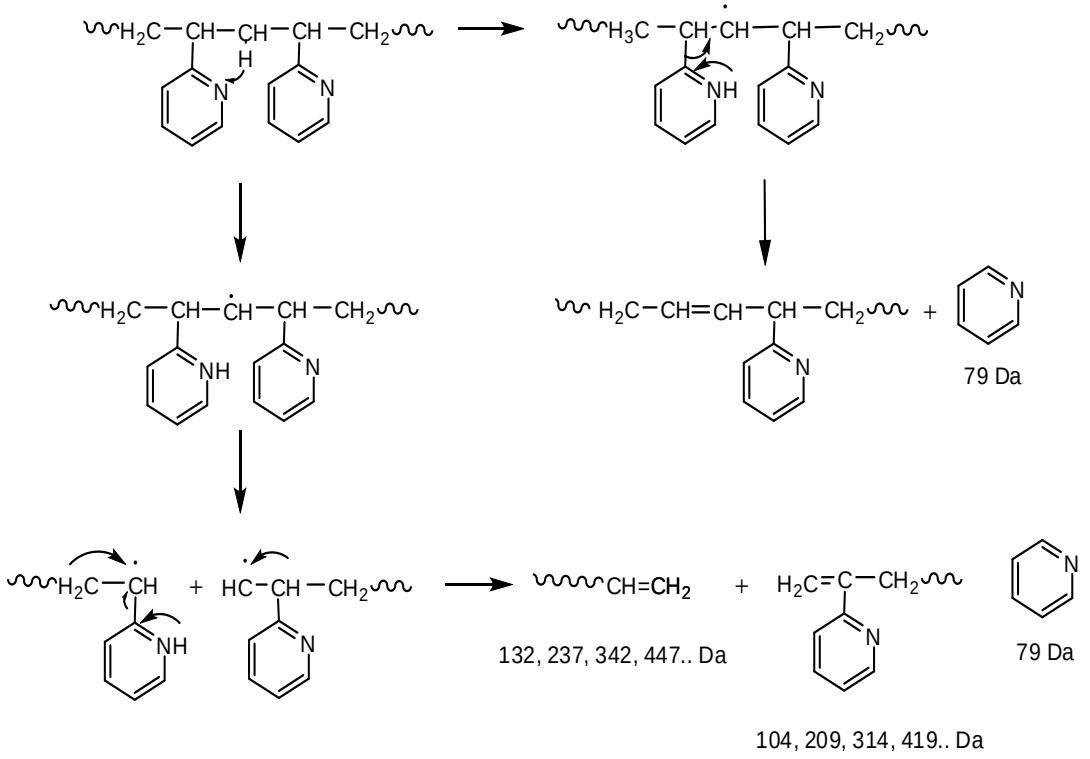

For the polyisoprene block of the copolymer, fragmentation pattern is also known from the literature. The diagnostic thermal degradation products of the isoprene block such as $C_5H_8^+$ (monomer) at 68 Da, $C_6H_9^+$ at 81 Da, $C_7H_{12}^+$ at 96 Da, $C_{10}H_{16}^+$ (dimer) at 136 Da,$C_{15}H_{24}^+$ (trimer) at 204 Da, and $C_{19}H_{30}^+$ at 258 Da were proposed to be generated by α and β scissions to the double bonds accompanied by hydrogen transfer reactions [48]

Scheme 4.2. Thermal degradation mechanism of polyisoprene

a.

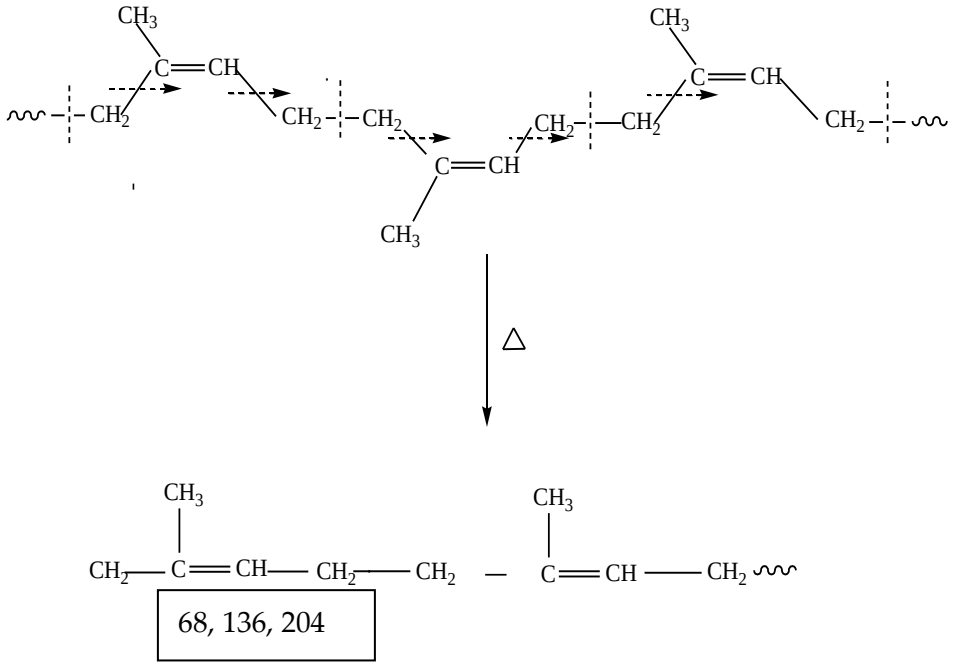

b.

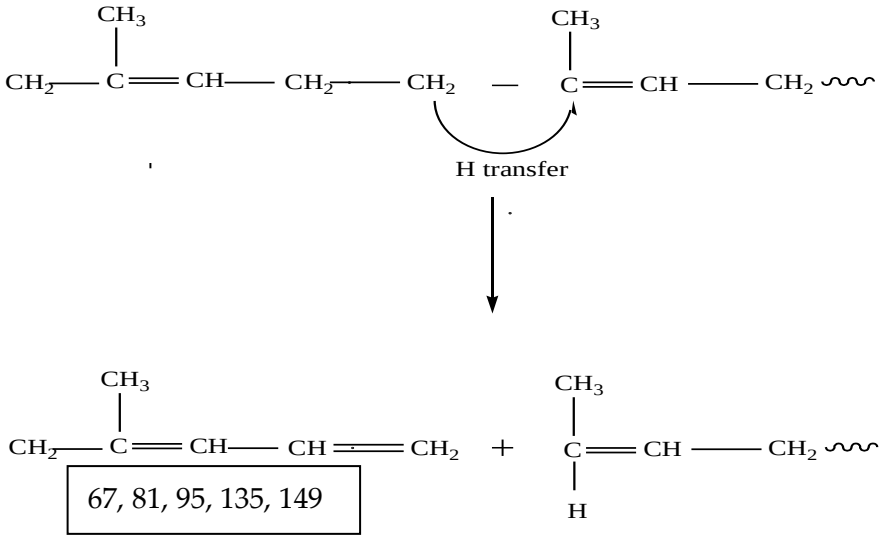

A thermal degradation characteristic of PI-b-P2VP was studied via DP-MS technique for the first time in this study. The total ion current (TIC) curve that is the variation of total ion yield as a function of temperature recorded during the pyrolysis of polyisoprene-block-poly2vinylpyridine, PI-b-P2VP is shown in Figure 4.13.

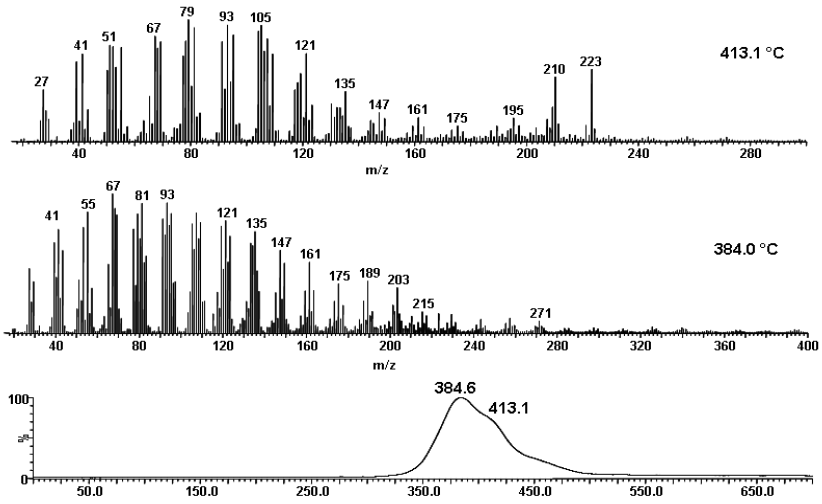

Figure 4.13. The TIC curve and the pyrolysis mass spectra recorded during pyrolysis of PI-b-P2VP

The relative intensities of the characteristic and/or intense peaks present in the pyrolysis mass spectra recorded at the peak maximum and at the shoulder present in TIC curve of the copolymer and the assignments made are summarized in Table 4.1. The peaks characteristic to PI block were more intense around 384°C, whereas those diagnostic to P2VP were maximized around 413°C indicating a higher thermal stability for the P2VP blocks. The MW of PI block was greater than that of P2VP block. Thus, the higher thermal stability can directly be attributed to presence of aromatic units.

Table 4.1. Peak assignments for PI-b-P2VP

m/z	Relative Intensities		Assignments
	384 °C	413 °C	
67	1000	868.8	$(M_{isoprene}\text{-}H)^+$
68	922.4	757.7	Isoprene monomer
77	760.0	710.1	$C_5H_3N^+$
79	880.3	1000	C_5NH_5
81	963.6	971.5	$C_5H_7\text{-}CH_2^+$
82	531.5	205.8	$C_5H_7\text{-}CH_3^+$
91	841.5	827.7	$C_7H_7^+$
93	920.8	955.6	$C_6H_6NH^+$
95	913.8	876.8	$C_6H_9\text{-}CH_2^+$
105	817.3	962.4	$C_7H_7\text{-}N^+$ (VP monomer)
118	195.6	491.3	$M_{VP}CH^+$
121	835.1	720.8	$CH_2{=}C(CH_3)\text{-}\ CH_2\text{-}CH_2\text{-}\ C(CH_3){=}CH^+$
135	759.8	409.0	D-H (Isoprene Dimer)
136	434.0	434.0	Isoprene Dimer
144	75.7	176.3	$M_{VP}C_3H_3^+$
203	331.0	114.3	T-H(Isoprene Trimer)
204	139.1	46.4	Isoprene Trimer
210	134.7	540.4	VP Dimer
218	38.2	38.2	$(CH_2\text{-}C(CH_3){=}\ CH\text{-}CH_2)_3{=}CH_2^+$
223	160.0	612.6	DCH (VP Dimer)

In order to a better understand single ionevolution profiles of characteristic fragments of each block are studied. In Figure 4.14. some selected examples namely, $C_5H_7^+$ at m/z=67 Da and $C_{19}H_{29}^+$ at m/z= 257 for the PI block and 2-vinyl pyridine monomer and dimer at m/z= 105 and 210 respectively and the protonated dimer at m/z=211 Da for the P2VP block are shown. The yields of products due to decomposition of PI block were maximized at around 282 °C, those of P2VP oligomers were maximized at 411 °C. The protonated oligomers of P2VP reached to maximum yield at slightly higher temperatures at around 419 °C in accordance to literature results [18].

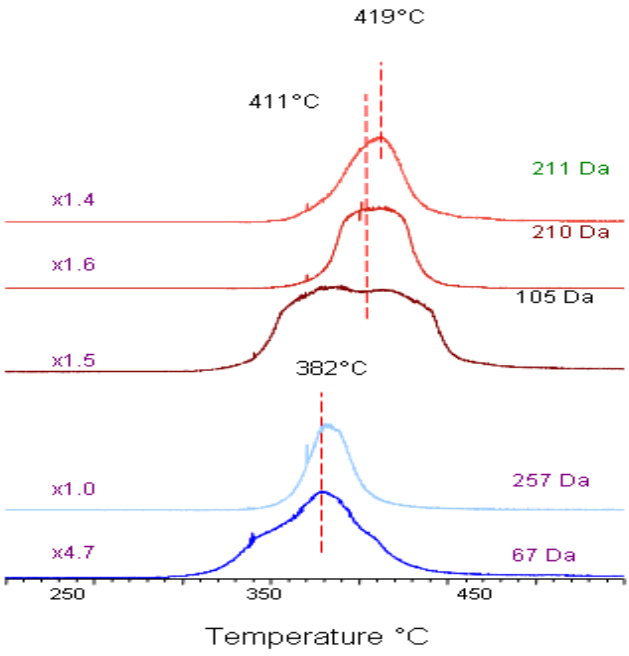

Figure 4.14 . Single ion evolution profiles of some selected thermal decomposition products recorded during the pyrolysis of PI-b-P2VP

4.4.1.1. Cr-(PI-b-P2VP)

Direct pyrolysis mass spectrometry analysis of Cr-bonded diblock copolymer, Cr-(PI-b-P2VP) yielded a TIC curve with two well separated peaks (Figure 4.15.). The pyrolysis mass spectra recorded at the peak maxima are also included in the figure. Table 4.2. shows the relative intensities and the assignments made for the intense and/or characteristic peaks for the Cr-bonded copolymer Cr-(PI-b-P2VP).

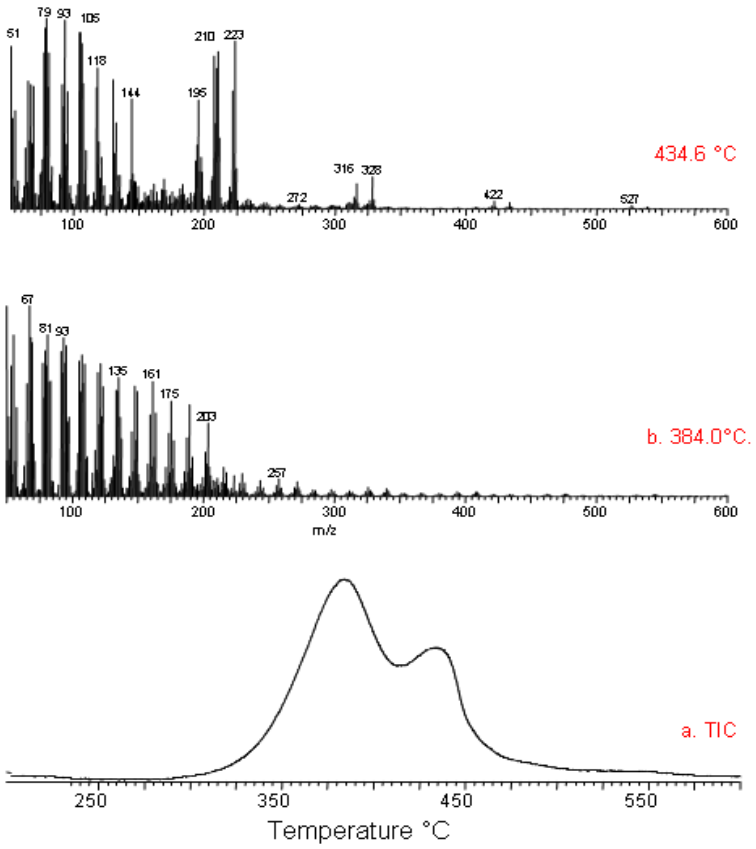

Figure 4.15. The TIC curve and the pyrolysis mass spectra recorded during pyrolysis of Cr-(PI-b-P2VP)

Table 4.2. Peak assignments for Cr-(PI-b-P2VP)

m/z	Relative Intensities		Assignments
	384 °C	434 °C	
67	1000	653.0	$(M_{isoprene}\text{-}H)^+$
68	834.3	343.7	Isoprene monomer
78	518.0	951.0	C_5NH_4, C_6H_6
79	765.0	1000	$C_5NH_5^+$
81	848.5	819.0	$C_5H_7\text{-}CH_2^+$
91	761.9	653.0	$C_7H_7^+$
93	833.2	992.1	$C_6H_6NH^+$
95	791.8	616.5	$C_6H_9\text{-}CH_2^+$
96	391.6	82.3	$C_6H_9\text{-}CH_3^+$
105	710.5	926.0	$C_7H_7\text{-}N^+$ (VP monomer)
121	697.2	272.1	$CH_2{=}C(CH_3)\text{-}\ CH_2\text{-}CH_2\text{-}\ C(CH_3){=}CH^+$
135	623.5	177.8	$CH_2\text{-}C(CH_3)\text{-}\ CH_2\text{-}\ CH_2\text{-}\ C(CH_3)\text{-}CH\text{-}CH_2$
136	415.9	51.5	Isoprene Dimer
144	84.8	577.1	$M_{VP}C_3H_3^+$
204	153.9	43.2	Isoprene Trimer
207	84.3	802	$C_{16}H_{15}$
210	96.6	826.2	Vinylpyridine Dimer
218	40.1	46.0	$(CH_2\text{-}C(CH_3){=}\ CH\text{-}CH_2)_3{=}CH_2^+$
223	108.8	880.4	$VP_D\text{-}CH$
237	12.2	29.1	$T_{VP}\text{-}Py^+$
281	17.5	17.2	$C_{22}H_{17}^+$
328	31.3	169.0	$C_{25}H_{28}^+$
401	1.4	2.4	$C_{31}H_{29}^+$

Upon coordination to metal significant changes in the pyrolysis mass spectra of the copolymer were detected. Intense peaks at 144 ($M_{VP}C_3H_3^+$) and 207 Da ($C_{16}H_{15}$) and moderate peaks at 281 ($C_{22}H_{17}$) and 328 Da ($C_{25}H_{28}$) appeared in the spectra. The single ion evolution profiles of the same characteristic fragments of each block discussed for the copolymer namely, $C_5H_7^+$ at m/z=67 Da and $C_{19}H_{29}^+$ at m/z 257 Da for the PI block and 2-vinyl pyridine monomer and dimer at m/z= 105 and 210 Da respectively and the protonated dimer at m/z=211 Da for the P2VP block are shown in Figure 4.16. The evolution profiles of $C_{16}H_{15}$ (m/z=207 Da) , $C_{22}H_{17}$ (m/z=281 Da) and $C_{31}H_{29}$ (m/z= 401 Da) are also included in the figure. The evolution profiles of PI based products showed a single peak with a maximum at around 385°C. The trends in the evolution profiles of these products are almost identical to the virgin copolymer. On the other hand, drastic changes were detected for P2VP based products. Two peaks with maxima at around 385 and 436°C were present in the evolution profile of 2VP monomer. The evolution profiles of the oligomers and protonated oligomers showed an intense peak with a maximum at around 436°C. A shoulder at around 385°C was also present in the evolution profiles of protonated oligomers. Furthermore, decrease in the yields of the protonated oligomers of 2VP was detected; i.e. protonated dimer yield decreased about 3 folds. Thus, structural changes in the P2VP chains causing increase in thermal stability were detected. Evolutions of products such as $C_{16}H_{15}$, $C_{16}H_{15}$ (m/z=207 Da) , $C_{22}H_{17}$ (m/z=281 Da) and $C_{31}H_{29}$ (m/z= 401 Da) involving H defficiency showed maximum also at around 436°C. Some of these products showed a second maximum at around 447 °C. It may be thought that these products were produced during the thermal degradation of the polymeric backbone generated upon lose of pyridine units coordinated to Cr metal in accordance with our previous result obtained for Cr-PS-b-P2VP [49]. Thus, it can be concluded that upon coordination of Cr to N of the pyridine ring, thermal degradation mechanism changes; either conjugated double bonds or a crosslinked

structure (C_xH_y where x≥y) due to the intermolecular coupling reactions between the main chains of P2VP can be formed (Scheme 4.3). In addition, polyene molecules may undergo Diels–Alder reaction, yielding six-membered rings along the polymer chain.

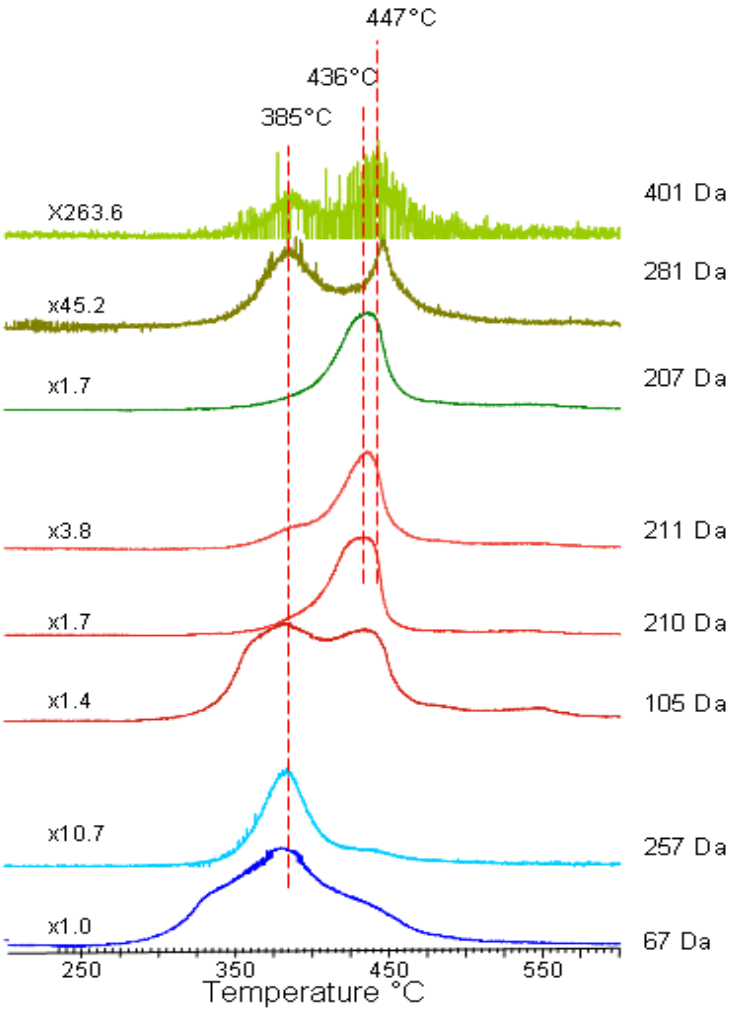

Figure 4.16. Single ion evolution profiles of some selected thermal decomposition products recorded during the pyrolysis of Cr-(PI-b-P2VP)

Scheme 4.3. Thermal degradation mechanism of metal-coordinated copolymer

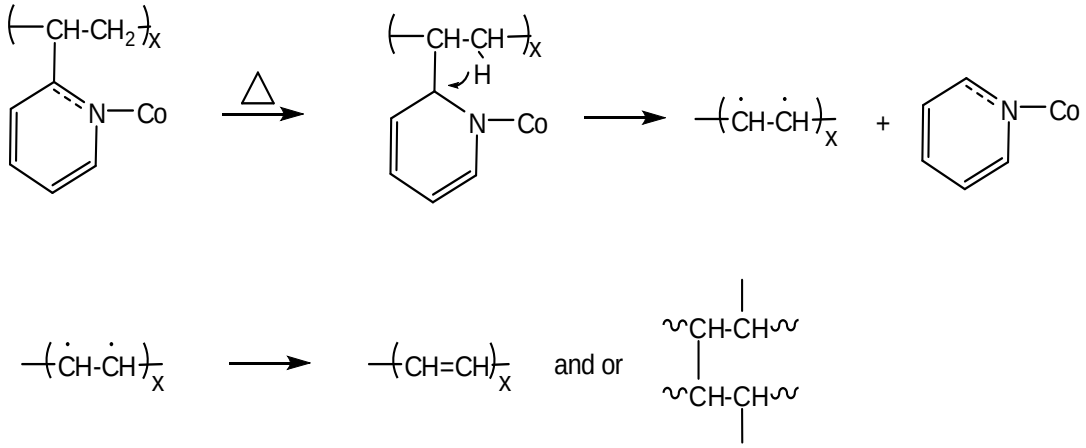

In summary, thermal degradation of units coordinated to metal losses pyridine units in the first step generating an unsaturated or crosslinked polymer backbone. This polymer backbone decomposes at higher temperatures yielding fragments involving H-deficiency such as products with m/z values 207, 281, 328 and 401 Da.

4.4.1.2. Au^{3+} -(PI-b-P2VP)

The TIC curve and the pyrolysis mass spectra at the peak maxima at 379.6 ^{o}C and the shoulder at 445 ^{o}C recorded during the pyrolysis of Au^{3+}-bonded (PI-b-P2VP) are shown in Figure 4.17.

The changes in the mass spectra recorded in the region where P2VP based products evolved were more significant. It can be noted from the figure that intense peaks at 210 (VP dimer) and 223 Da due to P2VP based products, diminished drastically.

Table 4.3. shows the relative intensities and the assignments made for the intense and/or characteristic peaks for the metal-bonded copolymer Au^{3+} - PI-b-P2VP

Around 250 °C, evolution of HCl was detected. But in this region no peak that can be attributed to decomposition of polymer was recorded.

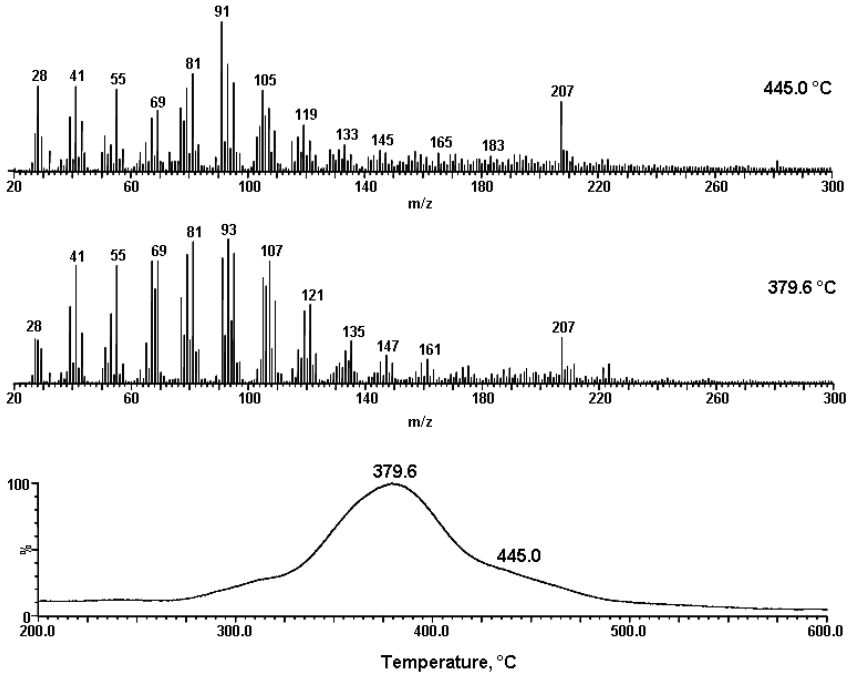

Figure 4.17. The TIC curve and the pyrolysis mass spectra recorded during pyrolysis of Au^{3+}-(PI-b-P2VP)

Table 4.3. Peak assignments for Au^{3+}-(PI-b-P2VP)

m/z	Relative Intensities		Assignments
	380 °C	**445 °C**	
67	846.8	284.7	$(M_{isoprene}\text{-}H)^+$
79	892.0	448.1	$C_5H_5N^+$
81	981.1	520.6	$C_5H_7N^+$
91	870.6	681.8	$C_6H_5N^+$
93	1000	572.7	$C_5H_7C_2H_2^+$
95	902.0	436.1	$C_6H_9\text{-}CH_2^+$
105	732.0	417.5	$C_7H_7\text{-}N^+$ (VP monomer)
107	849.8	330.8	$C_5H_7C_3H_4^+$
119	500.7	236.3	$M_{VP}CH_2^+$
121	544.8	159.4	$CH_2{=}C(CH_3)\text{-}\ CH_2\text{-}CH_2\text{-}\ C(CH_3){=}CH^+$
136	77.3	24.3	Isoprene Dimer
144	65.4	51.8	$M_{VP}C_3H_3^+$
204	33.7	22.5	Isoprene Trimer
207	290.8	296.1	$C_{16}H_{15}^+$
210	30.2	47.0	VP Dimer
217	36.5	29.7	$(CH_2\text{-}C(CH_3){=}\ CH\text{-}CH_2)_3{=}CH^+$
223	130.6	58.2	VP DCH
281	11.4	35.0	$C_{22}H_{17}^+$
315	9.0	11.9	T_{VP}^+
316	48.0	21.3	$T_{VP}H^+$
401	2.4	7.0	$C_{31}H_{29}^+$
420	3.2	4.6	$Te_{(VP)}^+$
421	25.5	8.7	$Te_{(VP)}H$

Changes in the relative intensities of P2VP based peaks were noted around 380°C. Relative intensities of the monomer and the dimer peak of 2VP decreased while the relative intensity of 207 Da ($C_{16}H_{15}^{+}$) peak increased significantly upon coordination to Au^{3+}. Single ion evolution profiles of characteristic fragments of each block namely, $C_5H_7^{+}$ at m/z=67 Da and $C_{19}H_{29}^{+}$ at m/z 257 Da for the PI block and 2-vinyl pyridine monomer and dimer at m/z= 105 and 210 Da respectively and the protonated dimer at m/z=211 Da for the P2VP block and the fragments with m/z values 207, 281 and 401 Da are shown in Figure 4.18.

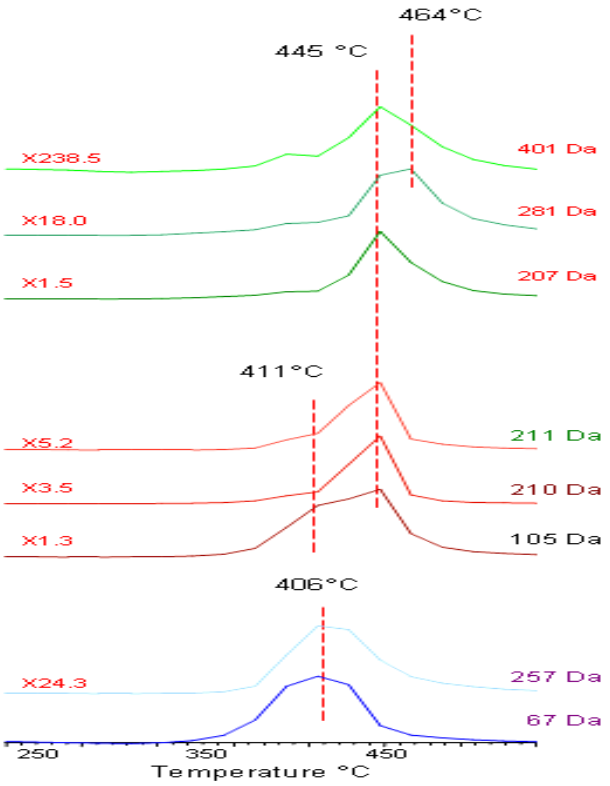

Figure 4.18. Single ion evolution profiles of some selected thermal decomposition products recorded during the pyrolysis of Au^{3+}-PI-b-P2VP

The evolution profiles of PI based products showed a single peak with a maximum at around 406°C. Thus, again, only a slight shift to high temperatures was detected in the evolution profiles of these products. On the other hand, for P2VP based products, single ion pyrograms showed a maximum at around 445°C. The yields of the protonated oligomers of 2VP decreased more than those of the oligomers; i.e. dimer yield decreased only about 2 folds whereas protonated dimer yield decreased about 3 folds. A second maximum at around 464°C was detected for some of the H-deficient products. The pyrolysis mass spectrometry analysis indicated, similar structural changes in the P2VP chain upon coordination to Au^{3+} increasing the thermal stability of P2VP chains. Relative yields of products involving H-deficiency were more intense for this sample. Thus, a similar thermal decomposition mechanism for the units involving metal ion coordination as shown in Scheme 4.3. can be proposed. However, taking into account the trends in evolution profiles, it can be concluded that upon coordination to Au^{3+}, a thermally more stable polymer was obtained.

4.4.1. Cr and Au^{3+} functional poly(methyl methacrylate)-block-poly(2-vinylpyridine)

As previously stated, the mass spectral data for the P2VP blocks of the copolymer shows that the thermal degradation of the block occurs via radicallic depolymerization yielding mainly vinylpyridine monomer, loss of pyridine and by proton transfer to N atom from the main chain yielding unsaturated linkages on the polymer backbone which in turn increases thermal stability. It is known that poly(methyl methacrylate), (PMMA), degrades via a mixture of chain end and random chain scission initiation followed by depropagation which produces mostly monomer and low molecular weight oligomers as shown in Scheme 4.4.[50]

Scheme 4.4. Thermal degradation mechanism of Poly(methyl methacrylate)

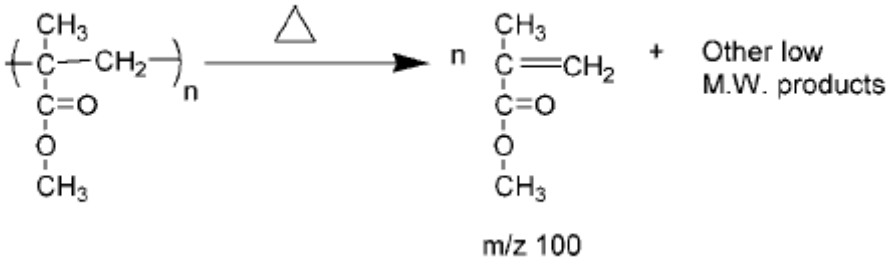

Thermal degradation behavior of poly(methyl metacrylate)-block-poly(2-vinylpyridine), PMMA-b-P2VP was studied via DP-MS technique for the first time in this study. The total ion current (TIC) curve recorded during the pyrolysis of PMMA-b-P2VP is shown in Figure 4.19. A broad single peak was recorded. PMMA

based peaks were relatively more intense as expected from the molecular weight distribution of the copolymer. Table 4.4. shows the relative intensities and the assignments made for the intense and/or characteristic peaks for the metal-bonded copolymer PMMA-b-P2VP.

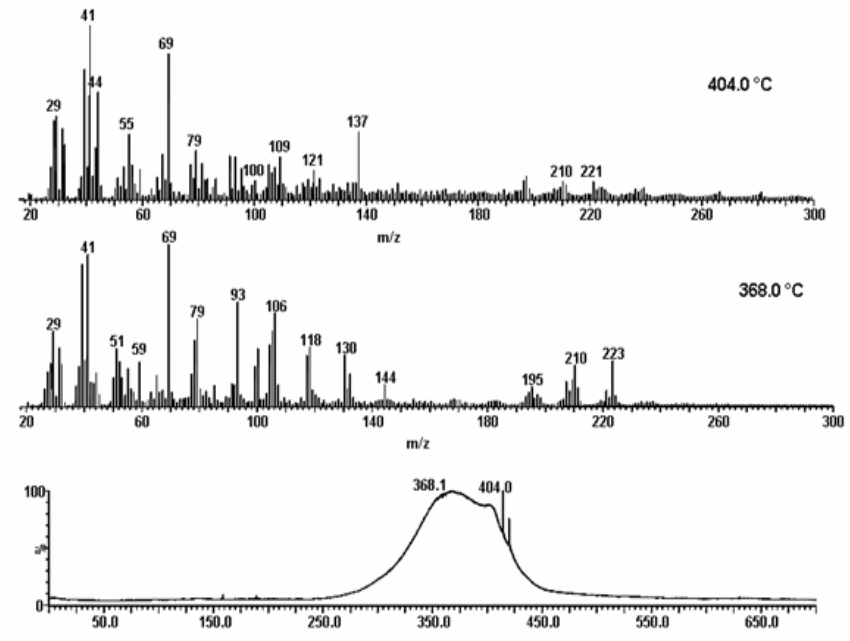

Figure 4.19. The TIC curve and the pyrolysis mass spectra recorded during pyrolysis of PMMA-b-P2VP

Table 4.4. Peak assignments for PMMA-b-P2VP

m/z	Relative Intensities		Assignments
	368 °C	404 °C	
41	938.1	1000	CH_2CCH_3
69	21.2	836.8	$CH_2C(CH_3)O$
77	194.7	198.0	$C_5H_3N^+$
78	407.7	118.7	$C_5H_4N^+$
79	537.6	278.0	$C_5H_5N^+$ Pyridine (Py)
91	136.9	245.6	$C_6H_5N^+$
93	643.4	241.7	$C_5H_7C_2H_2^+$
99	243.7	79.3	$CH_2C_3H_5COO(M_{MMA}-H)$
100	354.2	106.6	M_{MMA}
105	463.7	198.9	M_{VP}
106	577.3	151.1	$M_{VP}H$
118	365.8	69.9	$M_{VP}CH$
132	198.6	45.4	D_{VP}-Py
144	130.2	52.4	$M_{VP}C_3H_3$
195	116.8	49.3	D_{VP} -CH3
210	250.7	100.4	D_{VP}
211	112.8	80.2	$D_{VP}H$
223	278.0	62.9	$D_{VP}CH$
315	10.6	9.4	T_{VP}
316	28.2	16.9	$T_{VP}H$
420	1.1	0.7	$Te_{(VP)}$
421	1.5	3.9	$Te_{(VP)}H$

Single ion evolution profiles of some selected products are shown in Figure 4.20. As can be noted from the figure evolution of PMMA based products; CH_2CCH_3 (41 Da), $CH_2C(CH_3)O$ (69 Da) and the monomer (100 Da) occurred almost in the same temperature region with those of P2VP; monomer (105 Da), dimer (210 Da). Evolution of protonated oligomers of P2VP was observed at slightly higher temperatures in accordance with the thermal degradation of the homopolymer. Thermal decomposition products of P2VP were detected at lower temperatures compared to what was observed for the copolymer PI-b-P2VP. This behavior can be associated with significantly lower MW of P2VP block of PMMA-b-P2VP copolymer (4200) compared to PI-b-P2VP (23000).

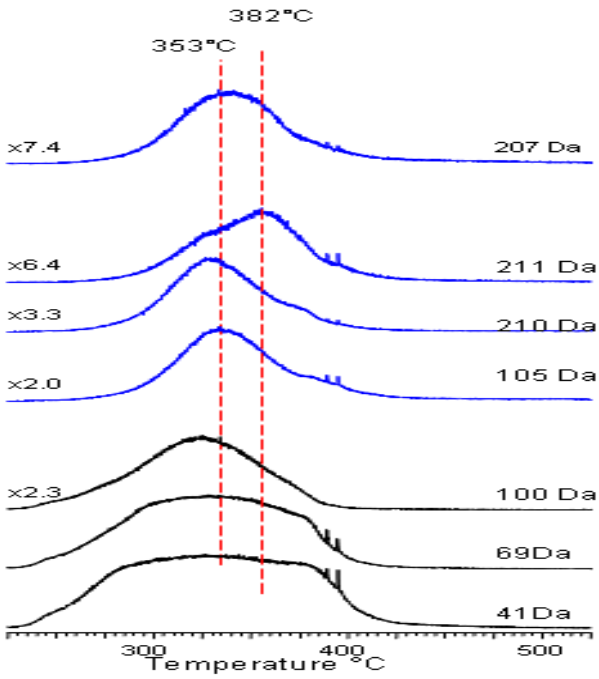

Figure 4.20. Single ion evolution profiles of some selected thermal decomposition products recorded during the pyrolysis of PMMA-b-P2VP

4.4.2.1. Cr- poly(methyl methacrylate)-block-poly(2-vinylpyridine)

The TIC curve and the pyrolysis mass spectra at 406.5 °C and at 425,5 °C recorded during the pyrolysis of chromium functional copolymer are shown in Figure 4.21. Pyrolysis mass spectra were dominated with PMMA based products. Again this may be related to composition of the copolymer. (MW of PMMA is 18700; MW of P2VP is 4200). Similar to PI-b-P2VP, decrease in the relative intensities of oligomer and protonated oligomer peaks of P2VP were detected. Table 4.5. shows the relative intensities and the assignments made for the intense and/or characteristic peaks for the Cr-bonded copolymer Cr-(PMMA-b-P2VP).

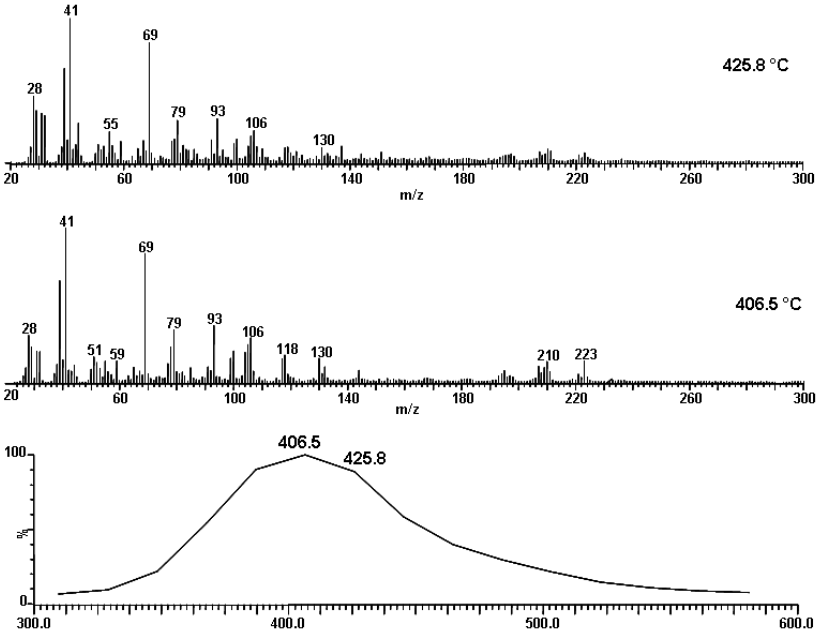

Figure 4.21. The TIC curve and the pyrolysis mass spectra recorded during pyrolysis of Cr-(PMMA-b-P2VP)

Table 4.5. Peak assignments for Cr-(PMMA-b-P2VP)

m/z	Relative Intensities		Assignments
	406 °C	425 °C	
39	659.2	655.4	C_3H_3
41	1000	1000	CH_2CCH_3
59	139.7	147.5	$COOCH_3$
69	834.2	832.5	$CH_2C(CH_3)O$
77	120.9	147.2	$C_5H_3N^+$, C_6H_5
78	228.0	162.8	$C_5H_4N^+$
79	337.6	292.5	$C_5H_5N^+$
91	101.5	157.7	$C_6H_5N^+$
93	368.8	304.5	$C_5H_7C_2H_2^+$
99	155.4	130.5	$CH_2C_3H_5COO(M_{MMA}-H)$
100	204.5	165.2	M_{MMA}
105	243.8	186.4	M_{VP}
106	289.1	222.6	$M_{VP}H$
118	177.3	107.4	$M_{VP}CH$
132	99.9	64.2	D_{VP}-Py
144	78.4	61.1	$M_{VP}C_3H_3$
210	136.1	94.0	D_{VP}
211	70.7	81.8	$D_{VP}H$
223	140.1	67.7	$D_{VP}CH$
237	13.7	8.1	T_{VP}-Py
315	7.5	7.3	T_{VP}
316	21.0	14.2	$T_{VP}H$
342	3.7	4.4	$Te_{(VP)}$-Py
401	1.7	1.9	$C_{31}H_{29}$+
420	2.5	1.5	$Te_{(VP)}$

Single ion evolution profiles of some selected products namely, CH_2CCH_3 (41 Da), $CH_2C(CH_3)O$ (69 Da), MMA monomer (100 Da), VP monomer (105 Da), VP Dimer (210 Da), protonated VP dimer (211 Da), $C_{16}H_{15}^+$ (207 Da), $C_{22}H_{17}^+$ (281 Da), $C_{31}H_{29}^+$ (401 Da) are shown in Figure 4.22. As can be noted from the figure, single ion evolution profiles of PMMA based products showed almost the same trends with those for the virgin copolymer. On the other hand, single ion evolution profiles of P2VP based products shifted to high temperatures. The maximum for the evolution profiles of P2VP based products for the virgin copolymer was 353 °C, whereas, for Cr-(PMMA-b-P2VP), it was at 406 °C.

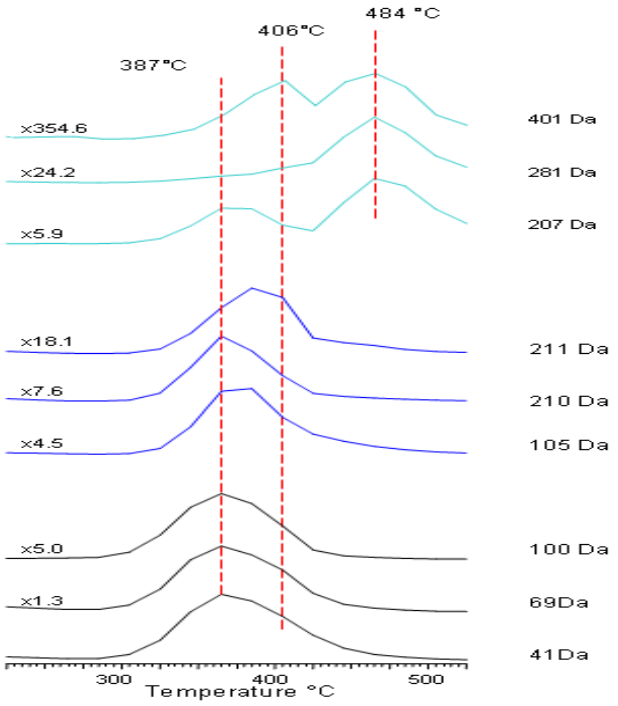

Figure 4.22. Single ion evolution profiles of some selected thermal decomposition products recorded during the pyrolysis of Cr-(PMMA-b-P2VP)

Furthermore, in general, both PMMA and P2VP based product evolutions shifted to higher temperatures more than what was observed for PI-b-P2VP case. The relative yield of all PMMA and P2VP based products decreased compared to the base peak upon coordination of Cr to N. The decrease in the relative yield of pyridine was even more significant confirming coordination to metal. Thus, it can be thought that thermal behavior of PMMA affected more than PI in the presence of Cr. Products that can be attributed to H deficient fragments were observed at noticeably higher temperatures. A second peak at around 484 °C was present in the evolution profiles of these products.

4.4.2.2. Au^{3+}-Poly(2-vinylpyridine-block-methyl methacrylate)

The TIC curve and the pyrolysis mass spectra at the peak maxima, at 408.3 and 455.1 °C recorded during the pyrolysis of Au^{3+} functional PMMA-b-P2VP are shown in Figure4.23. Decrease in the relative intensities of high mass peaks was recorded. On the other hand, significant increase in relative intensities of the products attributed to fragments generated by thermal degradation of the polymer backbone formed upon lose of pyridine units coordinated to metal ion was observed. Table 4.6. shows the relative intensities and the assignments made for the intense and/or characteristic peaks for the Au^{3+}-bonded copolymer Au-(PMMA-b-P2VP)

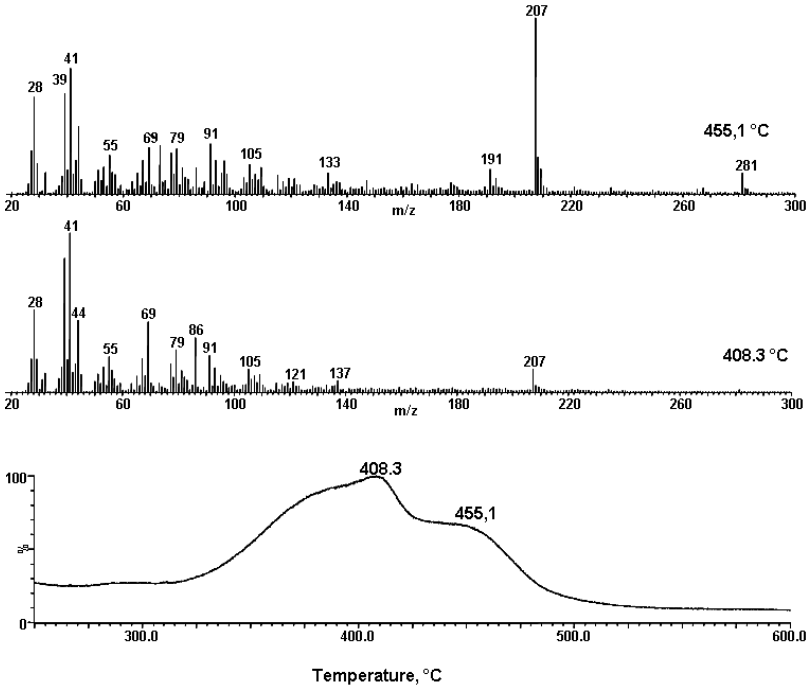

Figure 4.23. The TIC curve and the pyrolysis mass spectra recorded during pyrolysis of Au^{3+}-(PMMA-b-P2VP).

Table 4.6. Peak assignments for Au^{3+}-(PMMA-b-P2VP)

m/z	Relative Intensities		Assignments
	408 °C	**455 °C**	
36	21.7	18.8	
41	1000	823.9	$CH_2CCH_3^+$
69	442.6	293.1	$CH_2C(CH_3)O^+$
77	178.1	206.5	$C_5H_3N^+$
79	267.7	257.8	$C_5H_5N^+$
91	231.4	272.0	$C_6H_5N^+$
93	154.6	166.9	$C_5H_7C_2H_2^+$
100	46.2	16.0	M_{MMA}
105	144.9	160.2	M_{VP}
106	81.7	78.5	$M_{VP}H$
118	38.1	38.3	$M_{VP}CH$
132	17.1	21.7	D_{VP}-Py
144	22.5	24.3	$M_{VP}C_3H_3$
195	22.1	29.4	D_{VP} -CH3
207	148.3	694.0	$C_{16}H_{15}^+$
210	21.0	23.6	D_{VP}
211	20.1	26.9	$D_{VP}H$
223	18.5	21.0	$D_{VP}CH$
237	7.9	13.1	T_{VP}-Py
281	16.9	80.0	$C_{22}H_{17}^+$
315	2.6	2.3	T_{VP}
316	3.3	3.6	$T_{VP}H$
401	1.8	5.3	$C_{31}H_{29}^+$
421	1.3	1.7	$Te_{(VP)}H$

Single ion evolution profiles of some selected products namely, HCl (36 Da), CH_2CCH_3 (41 Da), $CH_2C(CH_3)O$ (69 Da), MMA monomer (100 Da), VP monomer (105 Da), VP dimer (210 Da), protonated VP dimer (211 Da), $C_{16}H_{15}$ (207 Da), $C_{22}H_{17}$ (281 Da), $C_{31}H_{29}$ (401 Da) are shown in Figure 4.24. Unlike the Cr functional PMMA-b-P2VP, evolution profiles of PMMA based products were also changed significantly. First of all, evolution HCl was detected at early stages of pyrolysis, around 210 °C. Slightly above this region, around 235 °C evolution of some PMMA and P2VP based products was also detected indicating degradation of both polymer chains most probably due to the effect of HCl evolution. Again, relative intensities of 2VP oligomer and protonated oligomer peaks decreased. But contrary to all other samples under investigation, significant decrease in the relative intensity of 2VP monomer peak was also detected. This behavior may be attributed to degradation of P2VP chains due to HCl evolution. But, as the relative yields of products associated with unsaturated and/or crosslinked polymer chains generated by lose of Au^{3+} coordinated pyridine units were noticeably high, it may be thought that the main reason for the decrease in the relative yield of P2VP based products was the extensive coordination of Au^{3+} for this sample. Another point that should be noticed was the change in the relative intensities of PMMA based products for this sample a high temperature peak in the evolution profile of MMA monomer, with a maximum at 484°C was present. It is clear that coordination of Au^{3+} to PMMA block also took place. It can be concluded that Au^{3+} can also coordinate to the carbonyl groups of MMA units ($CH_2C(CH_3)COOCH_3$). The lack of 69 and 41 Da peaks in this high temperature region pointed out the change in dissociative ionization mechanism when Au^{3+} coordinated to CO group.

Scheme 4.5. Thermal degradation mechanism of metal-coordination to PMMA-b-P2VP

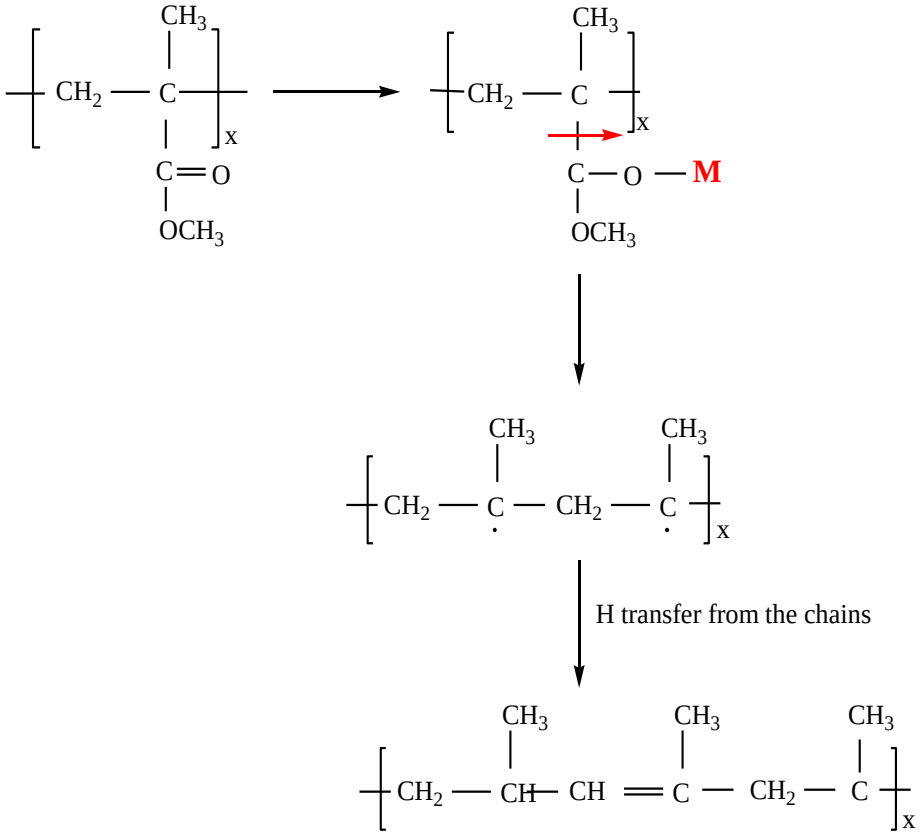

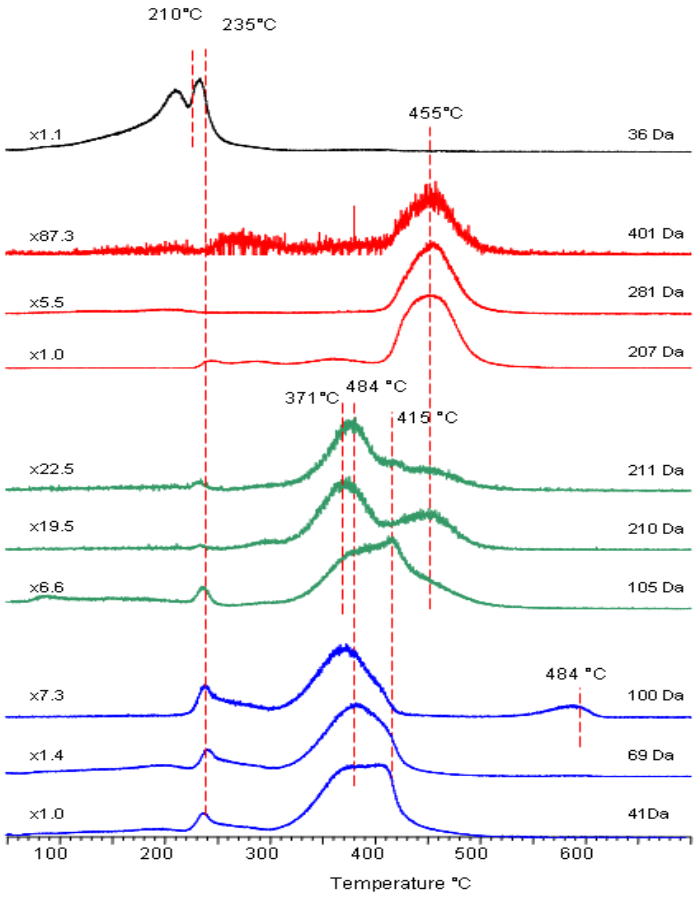

Figure 4.24. Single ion evolution profiles of some selected thermal decomposition products recorded during the pyrolysis of Au^{3+}-(PMMA-b-P2VP).

CHAPTER 5

CONCLUSIONS

In this work, the synthesis and characterization of nano structural chromium, Cr and gold(III), Au^{3+}, functional copolymers, polyisoprene-block-poly2vinylpyridine, (PI-b-P2VP) and poly2vinylpyridine-block-polymetylmethacrylate, (PMMA-b-P2VP) have been aimed. The effect of coordination of metal and metal ion on thermal characteristics of the copolymers was also investigated. For the purpose of characterization TEM, ATR-FT-IR, UV-Vis and Direct-Pyrolysis Mass Spectroscopy techniques were applied.

- Coordination of metal or/metal ion to the copolymers was confirmed by FT-IR, and UV-vis data. These results can be summarized as:

    - The sharp absorption peak at around 290 nm was attributed to a MLCT transition from chromium atom to π^* orbital of pyridine group in the UV-vis spectrum of the Cr-functional copolymers. Au-functional copolymers showed a completely new absorption band at around 320 nm which can be associated again with a LMCT transition. This behavior can be explained by electron deficient characteristic of Au^{3+}, more willing to accept electrons from the ligand.

- ATR-FT-IR spectrum of metal functional copolymers showed the disappearance of characteristic peaks of pyridine stretching and bending modes when metal coordinated to the pyridine nitrogen. Furthermore, the spectrum indicated the appearance of a new absorption which may be a clue for the coordination of metal or metal ion to the pyridine nitrogen. Additionally, in the spectrum of Au^{3+}-(PMMA-b-P2VP), the intensity of CO stretching peak of PMMA decreased while a new absorption peak appeared, revealing that the electron deficient gold (III) ion coordinated to both donor atoms present in the copolymer, namely CO of PMMA and nitrogen of P2VP in order to compensate its electron deficiency.

- Formation of nanostructures was confirmed by TEM analyses. The TEM images showed that the size Au^{3+} nanoparticles were 2 to 3 fold larger than that of Cr nanoparticles. Furthermore, micelle like structure formation was observed for Au^{3+} nanoparticles.

- The result of pyrolysis mass spectrometry analysis can be summarized as:

  - Coordination of Cr and Au^{3+} to N of pyridine units of poly(2- vinylpyridine) blocks of both copolymers increased the thermal behavior of these units in the range 30-50°C.

  - In general, coordination of Au^{3+} to copolymer increased the thermal stability more compared to what was detected for Cr coordination.

- In case of (PMMA-b-P2VP), besides the coordination of Au^{3+} to P2VP nitrogen atom extensively, coordination of electron deficient Au^{3+}, also to PMMA carbonyl group resulting drastic changes thermal stability of PMMA based products was also observed.

- In general, the increase in thermal stability was greater for PMMA-b-P2VP upon coordination to both Cr and Au^{3+}. It may be thought that the effect of increase in molecular weight is greater for low MW chains.

REFERENCES

1. Förster, S., Konrad, M., ***J. Mater. Chem.,*** 2003, **13**, 2671-1688
2. Ciebien, J.F., Clay, R.T., Sohn, B.H.,Cohen, R.E., ***New J. Chem.,*** 1998, 685-691
3. Haryono, A., Binder, W.F., ***Small***, 2006, 2, No. 5, 600-611
4. Wolfikis, website, last accessed date: 18 May 2009, ***Nanoparticles,*** http://wikis.lib.ncsu.edu/index.php/Nanoparticles
5. Diaz, C.,Valenzuela, M.L., ***J. Inorg. And Org. Polym. And Mater.,*** 2006, **16**, No. 2, 123-128
6. Park, C. *et al*, ***Polym.***, 2003, **44**, 6725-6760
7. Grubbs, R.B., ***J. Polym. Sci. Part A: Polym. Chem.,*** 2005, **43,** 4323-4330
8. Hashimoto, T., Harada, M., Sakamoto, N., ***Macro.,*** 1999, **32**, 6867-6870
9. Tadd, E. T. et al., **Mat. Res. Soc. Symo. Proc**., 2002, 703, 33-42
10. Bronstein, L. M.; Chernyshov, D. M.; Volkov, I. O.; Ezernitskaya, M. G.; Valetsky, P. M.; Matveeva,V. G.; Sulman, ***E. M. J Catal.,*** 2000, **196**, 302–314.
11. Platonova, O. A.; Bronstein, L. M.; Solodovnikov,S. P.; Yanovskaya, I. M.; Obolonkova, E. S.;Valetsky, P. M.; Wenz, E.; Antonietti, M., ***Coll. Polym Sci.,*** 1997, **275**, 426–431.
12. Diana, F. S.; Lee, S.-H.; Petroff, P. M.; Kramer,. *J. Nano Lett.,* 2003, **3**, 891–895.
13. Yoo, S. I.; Sohn, B.-H.; Zin, W.-C.; An, S.-J.; Yi,G.-C., ***Chem. Commun.,*** 2004, 2850–2851.
14. Sohn, B.-H.; Seo, B.-W., ***Chem. Mater.,*** 2001, **13**, 1752–1757.
15. Glass, R.; Moeller, M.; Spatz, ***J. P. Nanotech.,*** 2003, **14**, 1153–1160.
16. Moeller, M.; Spatz, ***J. P. Curr Opin Coll. Int. Sci***, 1997, **2**, 177–187.
17. Kaleli, K., "Nano Structural Metal Composites: Synthesis, Structural and Thermal Characterization", *Master of Science Thesis*, Middle East Technical University, Graduate School of Natural and Applied Science, Department of Chemistry, 2008

18. Elmacı, A.,''Thermal Characterization of Homopolymers, Copolymers and Metal Functional copolymers of Vinylpyridines'' *Master of Science Thesis*, Middle East Technical University, Graduate School of Natural and Applied Science, Polymer Science and Technology, 2008

19. Organometallic Hyper Text book, website, ***Carbonyl Complexes,*** http://www.ilpi.com/organomet/carbonyl.html, last accessed date: 20 June 2009

20. Wikipedia, the Free Encyclopedia, website, ***Metal Carbonyl,*** http://en.wikipedia.org/wiki/Metal_carbonyl, last accessed date:20 June 2009

21. Mason, W. R., Gray, H. B., ***J. Am. Chem. Soc.***,1968, 90(21), 5721-5729

22. Mason, W. R., Gray, H. B., ***Inorg. Chem.***,1968, 7 (1), 55-58

23. Tong, M.M., Berwer, D.G., ***Can. J. Chem.***, 1971, **49,(102)**

24. Skoog, D.A., Holler, F.J., Nieman, T.A.,***Princ. of Inst. Anal.,*** **5th edition**,1998

25. Hacaloğlu, J., Fares, M.M., Süzer, Ş., ***Euro. Polym. J.***, 1997, 939

26. Fares, M.M., Yalçın, T.,Hacaloğlu, J., Güngör, A., Süzer, Ş., ***Analyst***, 1994, 693

27. Qian, K., Killinger, W.E., Casey, M., ***Anal. Chem.,*** 1996, **68**, 1019-1027

28. Blazso, M***., J. Anal. Appl. Pyrolysis,*** 1997, **39**, 1-25

29. Tsuge, S., Ohtani, H., ***Polym. Deg. Stab.,*** 1997, **58**, 109-130

30. Prsi, Z., Gorecki, T., Poerschmann, J., ***J. Anal. Appl. Pyrolysis***, 2005, **74**, 11-18

31. Wapler, T., ***J. Anal. Appl. Pyrolysis***, 2004, **71**, 1-12

32. Lattimer, R.P., ***J. Anal. Appl. Pyrolysis***, 1997, **39**, 115-127

33. Baranauskas, V.V., Zalich, M.A., Saunders, M., St Pierre, T.G. Riffle, J.S., ***Chem. Mater.,*** 2005, **17**, 5246-5254

34. Hess, P., Parker, P.J., ***J. Appl. Polym. Sci.***, 1966, **10(12)**, 1915

35. Sastri, S.B., Armistead, J.P., Keller, T.M., Sorathia, U., **Polym. Compas.,** 1997, **18**, 48

36. Sastri, S.B., Keller, T.M., Sorathia, U., ***J. Appl. Polym. Sci.,*** 1998, **36**, 1885

37. Sumner, M.J., Sankarapandin, M., McGrath, J.E., Riffle, J.S., ***Polym.,*** 2002, 43, 5069

38. Tannenbaum, R., ***Inorg. Chim. Acta***, 1997, 227-233
39. Nogues, J., Schuller, J.K., ***J. Mag. Mater.,*** 1999, 192-203
40. Connolly, J., St. Pierre, T.G., Rutnakornpituk, M., Riffle, J.S., ***Eur. Cells Mater.,*** 2002, **3,** 106
41. Isci, H., Mason, W.R., ***Inorg. Chem.***,1983, **22**, 2266.
42. Schmidtke, H.H., Garthoff, D., ***J. Am. Chem. Soc.,*** 1967, **89**, 1317.
43. Paw, W., Cummings, S.D., Mansour, M.A., Connick, W.B., Geiger, D.K., Eisenberg, R., ***Coord. Chem. Rev.***, 1998, **171**, 125.
44. Mason, W.R., Gray, H. B.,***Inorg. Chem.,*** 1968, **7(1),** 55-58
45. Lu, J.Q., Yi,S.S., ***Lang.***, 2006, **22, No. 9,** 3951-3954
46. Bamba, T. *et. al.*, ***Int. Symp. Euc. Ulm.,*** 2007, **1, No. 1,** 109-111
47. Kumutha, K., Alias, Y., **Spect. Acta Part A,** 2006, **64**, 442–447
48. J. Hacaloglu et al., ***Euro. Polym. J.,*** 1999, **35**, 939-944
49. Elmaci, A., Hacaloglu J.,Kayran, C.,Sakellariou, G., Hadjichristidis, N., ***Polym. Deg. Stab.***, 2009 in press.
50. J. Hacaloglu et al., J. Mac. Sci., 2003, **A40, No. 6**, 605–615